Evidence for a nuclear role for *Drosophila* Dlg as a regulator of the NURF complex

Katherine A. Sharp[a], Mark J. Khoury[a], Frederick Wirtz-Peitz[b], and David Bilder[a,*]
[a]Department of Molecular and Cell Biology, University of California-Berkeley, Berkeley CA 94720; [b]Department of Genetics, Harvard Medical School, Boston, MA 02115

ABSTRACT **Scribble (Scrib), Discs-large (Dlg), and Lethal giant larvae (Lgl) are basolateral regulators of epithelial polarity and tumor suppressors whose molecular mechanisms of action remain unclear. We used proximity biotinylation to identify proteins localized near Dlg in the *Drosophila* wing imaginal disc epithelium. In addition to expected membrane- and cytoskeleton-associated protein classes, nuclear proteins were prevalent in the resulting mass spectrometry dataset, including all four members of the nucleosome remodeling factor (NURF) chromatin remodeling complex. Subcellular fractionation demonstrated a nuclear pool of Dlg and proximity ligation confirmed its position near the NURF complex. Genetic analysis showed that NURF activity is also required for the overgrowth of *dlg* tumors, and this growth suppression correlated with a reduction in Hippo pathway gene expression. Together, these data suggest a nuclear role for Dlg in regulating chromatin and transcription through a more direct mechanism than previously thought.**

Monitoring Editor
Richard Fehon
University of Chicago

Received: Apr 19, 2021
Revised: Aug 17, 2021
Accepted: Aug 30, 2021

INTRODUCTION

Discs-large (Dlg), Scribble (Scrib), and Lethal giant larvae (Lgl) are evolutionarily conserved polarity-regulating proteins found at the basolateral membranes of epithelial cells, where they restrict the localization of the aPKC and Par complexes to the apical region of the cell (Elsum *et al.*, 2012; Rodriguez-Boulan and Macara, 2014; Campanale *et al.*, 2017). They can also regulate the formation and maintenance of cell junctions, the division axis of epithelial cells, and the asymmetric division of stem cells (Woods *et al.*, 1996; Tepass and Tanentzapf, 2001; Albertson and Doe, 2003; Bilder *et al.*, 2003; Johnston *et al.*, 2009; Bergstralh *et al.*, 2013; Rodriguez-Boulan and Macara, 2014; Campanale *et al.*, 2017; Nakajima *et al.*, 2019). In *Drosophila* epithelia, loss of any one of these three proteins causes not only loss of polarity but also neoplastic transformation and tumorous overgrowth (Bilder *et al.*, 2000; Bilder, 2004; Hariharan and Bilder, 2006; Humbert *et al.*, 2008). Overgrowth results from an aberrant transcriptional program that is driven by Yorkie (Yki), the transcriptional activator of the Hippo pathway (Hariharan and Bilder, 2006; Grzeschik *et al.*, 2010; Zhu *et al.*, 2010; Doggett *et al.*, 2011; Sun and Irvine, 2011; Bunker *et al.*, 2015).

Dlg, Scrib, and Lgl are conserved in vertebrates where they each have multiple homologues (Elsum *et al.*, 2012). As in flies, the vertebrate proteins have been implicated in regulation of tumor growth, with changes detected in a variety of human cancers (Halaoui and McCaffrey, 2015). They are also involved in apicobasal polarity and formation of both adherens and occluding tight junctions in epithelial cells (Su *et al.*, 2012; Choi *et al.*, 2019) and have a similar role in endothelial cells (Elsum *et al.*, 2012; Lizama and Zovein, 2013; Worzfeld and Schwaninger, 2016). Further, Dlg homologues regulate the migration of epithelial cells during development. Mutations in these genes can result in cleft palate (Caruana and Bernstein, 2001), hydrocephalus (Nechiporuk *et al.*, 2007), and defects in renal and urogenital systems (Iizuka-Kogo *et al.*, 2007; Nechiporuk *et al.*, 2007; Elsum *et al.*, 2012).

Despite the importance of Scrib, Dlg, and Lgl for development, homeostasis, and disease, we still have a limited understanding of

This article was published online ahead of print in MBoC in Press (http://www.molbiolcell.org/cgi/doi/10.1091/mbc.E21-04-0187).

ORCID: Katherine A. Sharp: 0000-0002-7574-7331; Mark J. Khoury: 0000-0002-7211-0247; David Bilder: 0000-0002-1842-4966.

*Address correspondence to: David Bilder (bilder@berkeley.edu).

Abbreviations used: AED, after egg deposition; APEX2, enhanced ascorbate peroxidase 2; BSA, bovine serum albumin; Co-IP, coimmunoprecipitate; Dlg, Discs-large; E(bx), Enhancer of bithorax; FBS, fetal bovine serum; FDR, false discovery rate; GO, Gene Ontology; IP-MS, coimmunopreciptitation with mass spectrometry; Iswi, Imitation SWI; MAGUK, membrane-associated guanylate kinase; Lgl, Lethal giant larvae; MS, mass spectrometry; NES, nuclear export signal; NLS, nuclear localization signal; NURF, nucleosome remodeling factor; PBS, phosphate-buffered saline; PDZ, PSD95-Dlg-ZO-1 domain; PFA, paraformaldehyde; PLA, proximity ligation assay; Scrib, Scribble; SH3, Src homology 3 domain; SPS, synchronous precursor selection; TBS, Tris-buffered saline; TEAB, triethylammonium bicarbonate; TMT, tandem mass tag; Trl, Trithorax-like; Yki, Yorkie.

their molecular functions and the mechanisms by which they regulate cell biology and gene expression. Scrib and Dlg are multivalent "scaffolding" proteins containing a variety of protein–protein interaction domains and motifs. Scrib contains four PSD95-Dlg-ZO-1 (PDZ) domains and a leucine-rich repeat (LRR) domain, while Dlg contains three PDZ domains, one Src homology 3 (SH3) domain, and a catalytically dead guanylate kinase (GUK) domain (Tepass and Tanentzapf, 2001; Elsum *et al.*, 2012; Su *et al.*, 2012; Campanale *et al.*, 2017). Understanding the function of these scaffolds will require defining the proteins with which they interact as well as how those interactions change and are regulated over space and time within cells. However, PDZ and other domains are thought to facilitate weak and transient interactions, often involving plasma membrane (PM)-embedded receptors, making it difficult to define the full complement of proteins with which they interact using traditional biochemical methods (Amacher *et al.*, 2020). Numerous prior efforts have used coimmunopreciptitation with mass spectrometry (IP-MS) to identify binding partners for Dlg, Scrib, and Lgl (Audebert *et al.*, 2004; Van Campenhout *et al.*, 2011; Anastas *et al.*, 2012; Belotti *et al.*, 2013; Michaelis *et al.*, 2013; Nagasaka *et al.*, 2013; Ivarsson *et al.*, 2014; Waaijers *et al.*, 2016; Drew *et al.*, 2017; Dash *et al.*, 2018; Portela *et al.*, 2018; Nakajima *et al.*, 2019) (reviewed in Stephens *et al.*, 2018). However, such experiments have yielded largely nonoverlapping lists of binding partners and relatively few mechanistic insights. The limited utility of some IP-MS approaches may additionally derive from the use of nonepithelial cell lines in which functionally important interactions may not exist.

We sought a different approach that could be carried out in intact epithelial cells and that would not rely on strong, stable interactions between proteins. We therefore turned to proximity-based biotin labeling using the enhanced ascorbate peroxidase 2 (APEX2) enzyme. APEX2 is an ascorbate-peroxidase derived from the pea plant that, in the presence of hydrogen peroxide, catalyzes the conversion of phenol into a phenoxyl radical. In cells supplied with biotin-phenol as a substrate, APEX2 covalently labels proteins with biotin within a 20-nm radius of the enzyme (Figure 1A). By leveraging the strength and specificity of streptavidin-biotin binding, labeled proteins can then be efficiently and cleanly isolated and identified by MS (Martell *et al.*, 2012; Rhee *et al.*, 2013; Hung *et al.*, 2014, 2016; Lam *et al.*, 2014; Chen *et al.*, 2015). Proximity-based biotinylation has been used in a variety of experimental systems to identify catalogs of proteins associated with a particular organelle or localized to a particular subcellular region. Importantly, this method can also capture protein–protein interactions that cannot be isolated by more conventional methods (Rhee *et al.*, 2013; Van Itallie *et al.*, 2013; Hung *et al.*, 2014; Chen *et al.*, 2015; Gingras *et al.*, 2019; Mannix *et al.*, 2019; Trinkle-Mulcahy, 2019; Bagci *et al.*, 2020; Tan *et al.*, 2020).

As an entry point into understanding Scrib module function, we used an APEX2-tagged *Drosophila* Dlg to identify nearby proteins in an epithelium in vivo. In addition to previously proposed Dlg binding partners and other cortical proteins, there was a surprising enrichment of nuclear proteins, including the nucleosome remodeling factor (NURF) complex of chromatin regulators. We demonstrate that a nuclear pool of Dlg exists in proximity to NURF members and provide evidence that NURF facilitates the growth of *dlg* tumors by activating neoplastic transcriptional programs. Our results further demonstrate the utility of proximity-based proteomics for the elucidation of the localization and function of individual proteins, particularly for multivalent scaffolding proteins.

RESULTS

An APEX2-Dlg transgene for proteomics

To identify proteins enriched near Dlg in the cells of an intact epithelial sheet, we used APEX2-based in vivo proximity labeling. We drove an N-terminally tagged *UAS-3xMyc-APEX2-Dlg* (APEX2-Dlg) construct using a broadly but moderately expressed GAL4 driver (*D174-GAL4*) in a *dlg* null background. In these animals, APEX2-Dlg was the only Dlg protein present. APEX2-Dlg restored the morphology of *dlg* mutant discs (Figure 1, B, E, and H), and adult flies were rescued to viability and fertility (Figure 1, C, D, F, G, I, and J), demonstrating that this transgenic protein is fully functional. Because proximity-based proteomics labels not only direct binding partners but also all proteins within a 20-nm radius of the enzyme (Martell *et al.*, 2012) (Figure 1A), it is critical that APEX2-tagged constructs localize comparably to their wild-type counterparts. Comparison to endogenously tagged Dlg::EGFP revealed that APEX2-Dlg displayed similar localization along the basolateral membranes of wing disc epithelial cells (Figure 1, K and L). We tested the enzymatic function of APEX2-Dlg by treating both control and experimental discs with hydrogen peroxide and comparing the amount of biotinylation by Western blot. As expected, increased biotinylation was seen in lysate from discs expressing APEX2-Dlg as compared with control (Figure 1M), and we successfully isolated the biotinylated proteins using streptavidin beads from both control and experimental samples (Figure 1M and Supplemental Figure S1A). Finally, we assessed whether APEX2-Dlg would biotinylate proteins known to be in close proximity to endogenous Dlg. Indeed, Western blotting revealed that Scrib was present in the streptavidin-bead eluate from experimental but not control samples, verifying that APEX2-Dlg was functioning as designed (Figure 1N; Supplemental Figure S1B).

Proximity biotin labeling and MS analysis

We next collected samples from APEX2-Dlg epithelia for MS. Larvae were dissected to isolate the wing, haltere, and leg imaginal discs that are found together in the thorax. Samples were collected in batches, subjected to biotin labeling, and a small fraction of each postlabeling reaction lysate was reserved to verify consistent sample quality (Supplemental Figure S1, C and D). Batches were then pooled into three biological replicates for both the experimental and the control genotype, each containing the thoracic discs of 400 larvae. Samples were tandem mass tag (TMT) labeled and then pooled for LC-MS3 (see *Methods* for details).

The MS results yielded a list of 485 proteins with a *p* value below the statistical threshold and a log2 fold change of at least 2 between experimental and control samples (Supplemental Table S1). This list included many translation initiation and elongation factors as well as ribosomal proteins. It is possible that these proteins were labeled because APEX2-Dlg is translated from a UAS construct that is being continually produced. We therefore excluded them from further analysis, leaving a final dataset of 413 proteins (Supplemental Table S2).

We then performed cellular component Gene Ontology (GO) analysis on this dataset. Gratifyingly, enriched terms included "basolateral membrane" and "septate junction" (Figure 2, A and B). The proteins that led to these terms included both Scrib and Lgl, which function with Dlg in a module to regulate polarity, as well as Cora, Nrg, FasIII, Vari, and Atpα which are junctional components whose localization is regulated by Dlg (Woods *et al.*, 1996; Bilder *et al.*, 2003; Oshima and Fehon, 2011; Izumi and Furuse, 2014; Lee *et al.*, 2020). The dataset also included proteins previously identified as direct physical interactors of *Drosophila* Dlg (Kinesin heavy chain, Calmodulin Kinase II, 14-3-3 zeta and epsilon) (Koh *et al.*, 1999;

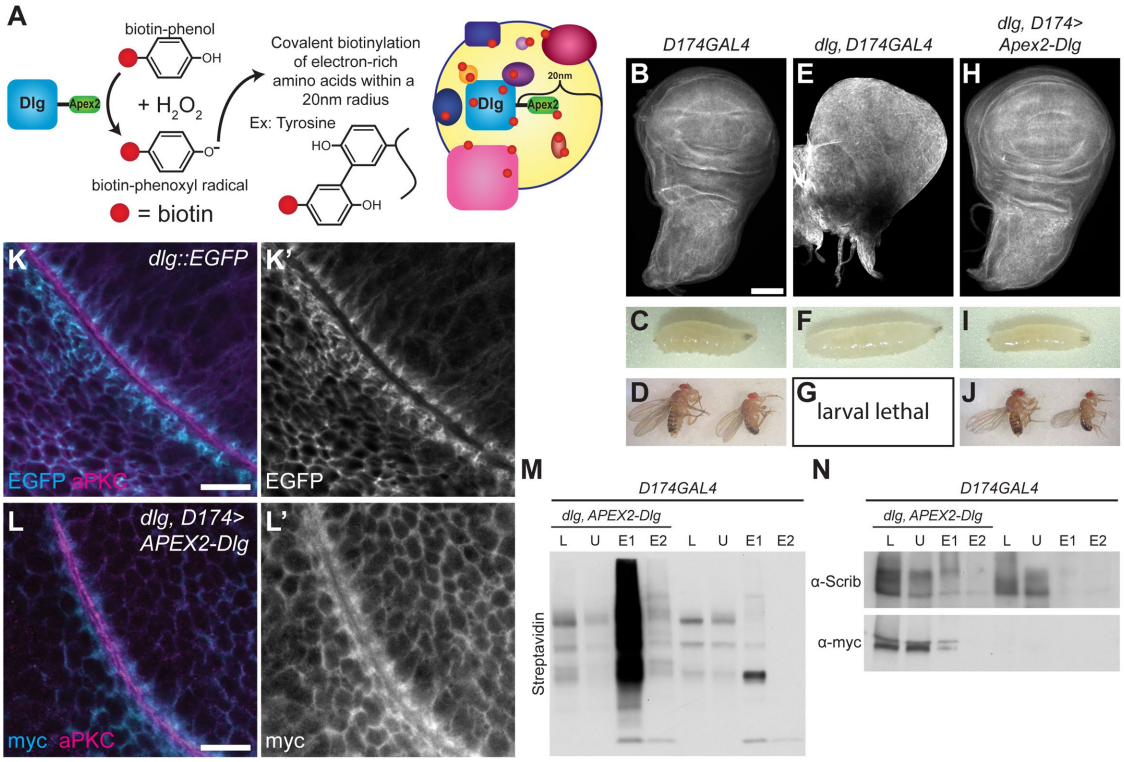

FIGURE 1: A fully functional APEX2-Dlg efficiently labels proteins with biotin. (A) In the presence of H_2O_2, APEX2 catalyzes the conversion of biotin-phenol into a phenoxyl radical that can then covalently label proteins with biotin within a 20 nm radius of the enzyme. (B–D) Control *D174GAL4* 3rd instar larval wing disc (B), larva (C), and adult (D) fly with normal size and morphology. Scale bar = 100 μM. (E–G) *dlg*, *D174GAL4* wing discs (E) form neoplastic tumors. Larvae (F) are overgrown and no adult flies eclose (G) because animals die as giant larvae. Scale bar = 100 μM. (H–J) *dlg* mutant phenotypes were rescued by *UAS-3xMyc-APEX2-Dlg* (*APEX2-Dlg*). Wing discs (H) have normal size and morphology, larvae are normal in size (I), and adult viability (J) and fertility are restored. Scale bar = 100 μM. (K) Endogenously tagged Dlg::EGFP reflects Dlg localization along the epithelial basolateral membrane of wing disc cells. Localization is excluded from the apical domain labeled by α-aPKC staining. Scale bar = 10 μM. (L) APEX2-Dlg (α-myc) localization recapitulated normal Dlg localization along the basolateral domain of wing disc cells and is excluded from the apical domain. Scale bar = 10 μM. (M) APEX2-Dlg efficiently labeled cellular proteins with biotin as seen by increased Streptavidin-HRP signal in experimental disc lysate (L, lane 1) compared with lysate from control discs (L, lane 5). Some biotinylated protein remained unbound to beads (U, lanes 2 and 6), but most was serially eluted off streptavidin–conjugated beads (eluate [E] 1 and 2, lanes 3, 4, 7, and 8). Biotinylation catalyzed by APEX2 was particularly apparent in these eluates. (N) Both experimental (lane 1) and control (lane 5) lysates (L) contained Scrib, but only experimental lysate contained APEX2-Dlg (α-myc). While some Scrib and APEX2-Dlg remained unbound (and possibly unlabeled) (U, lanes 2 and 5), both were detected in the experimental but not control streptavidin-bead eluate (E1, E2, lanes 3and 4 and 7 and 8) showing that both proteins were labeled with biotin only in the presence of the APEX2 tag.

Siegrist and Doe, 2005; Nakajima *et al.*, 2019). Other hits include the coassociated RNA binding proteins Caprin and Fmr1, the latter of which interacts with Lgl (Zarnescu *et al.*, 2005; Baumgartner *et al.*, 2013). Interestingly, "Proton-transporting V-type ATPase, V1 domain" is another enriched term in the GO analysis (Figure 2A and Supplemental Table S3), and a recent study identified an indirect physical interaction between the V-ATPase proton pump and the Lgl in cultured *Drosophila* cells (Portela *et al.*, 2018). Altogether, these results support the hypothesis that proximity-based proteomics can capture a snapshot of Dlg biology in living epithelia (Figure 2A and Supplemental Table S3).

Nuclear localization of Dlg

The GO analysis also highlighted some unexpected results. Proteins annotated to the term "nucleus" were enriched in the dataset (Figure 2, A and B; Supplemental Table S3). This was surprising because microscopy of fixed and immunostained tissue as well as live imaging with tagged fluorescent proteins detect Dlg localization almost exclusively at the basolateral membranes of epithelial cells (Figure 1, A and B). However, proteins associated with the GO-term "nuclear pore" were also overrepresented in the dataset and included proteins found in the pore's cytoplasmic filaments, the central ring which spans the nuclear envelope, and the nuclear basket (Nup358, Nup155, and Nup50 and Tpr; Figure 2, A and B; Supplemental Table S3). Proximity to these components is consistent with nuclear import of Dlg isoforms, all of which have molecular masses greater than 100 kDa.

We therefore investigated whether a nuclear pool of Dlg might exist in epithelia. We performed subcellular fractionation of wing disc lysates to generate nuclear and cytoplasmic fractions, validated by Western blotting for their canonical markers Lamin and Tubulin, respectively. Strikingly, a portion of Dlg is indeed found in the nuclear fraction (Figure 2C). It is not technically feasible to quantify the exact proportion of Dlg in the nucleus because of sample loss inherent to the fractionation protocol; however, taking into account the proportion of each fraction analyzed by Western blot (Figure 2C),

A

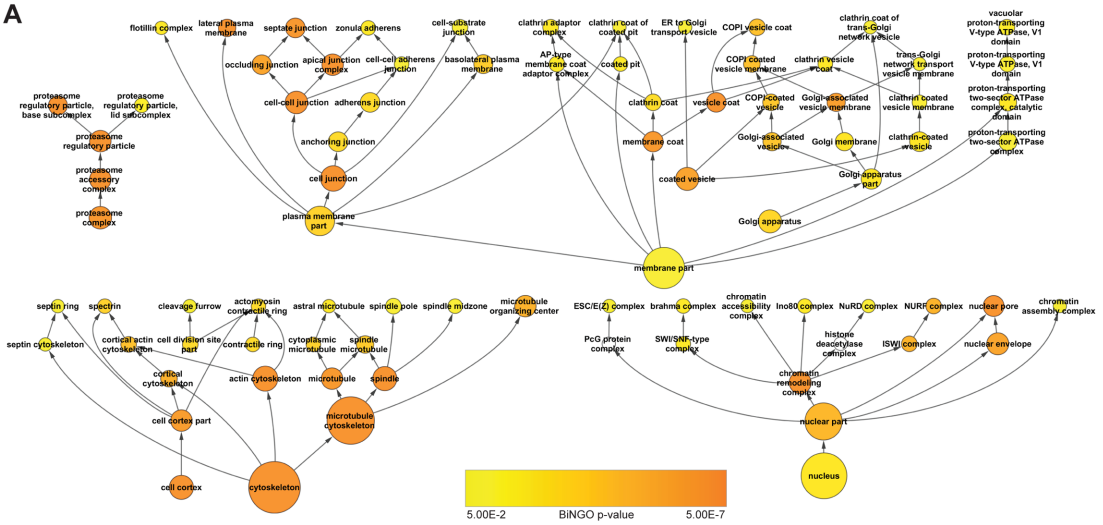

B

GO Terms- Cellular Component	P-value	Example genes
basolateral plasma membrane (GO:0016323)	1.91E-04	*dlg, alpha-Cat, Fas3, scrib, lgl, rhea, Zasp52, Actn*
septate junction (GO:0005918)	7.34E-07	*dlg, cora, Nrg, Fas3, scrib, lgl, vlc, Atpalpha, vari*
nuclear pore (GO:0005643)	1.82E-07	*Nup358, Nup154, Nup50, Mtor*
chromatin remodeling complex (GO:0016585)	2.89E-09	*pont, HDAC1, E(bx), brm, Iswi, Bap60, Caf1-55, Mi-2, Nurf-38*
NURF complex (GO:0016589)	1.56E-05	*E(bx), Iswi, Caf1-55, Nurf-38*

C

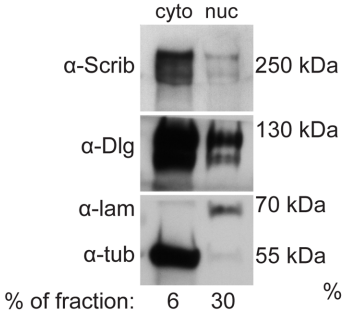

D

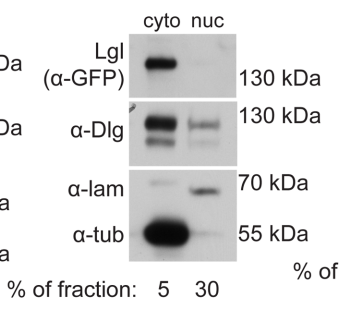

E

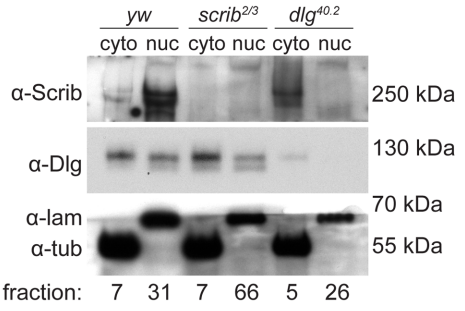

FIGURE 2: Existence of a nuclear pool of Dlg. (A) Hierarchical map of selected enriched cellular component GO terms from APEX2-Dlg proximity biotinylation. Size of circles indicates the number of genes associated with a given term. Color of the circle indicates the *p* value of enrichment for that term as indicated by the provided scale. Enriched terms include the proteasome; membrane-associated terms including regions of the cell, types of membrane associated proteins, and types of vesicles; cytoskeleton-related terms including actin and microtubule cytoskeletons; and nuclear terms. Map was pruned for viewability. Full list of enriched terms and their associated *p* values is found in Supplementary Table 3. (B) Selected enriched GO terms with their associated FDR-corrected *p* values, and examples of genes from the dataset associated with each term. "Basolateral PM" and "septate junction" were expected terms, while "nuclear pore," "chromatin remodeling complex," and "NURF complex" were unexpected. (C–E) Western blots of fractionated disc extracts, probed with Tubulin (α-tub) to mark the cytoplasmic fraction and Lamin (α-lam) to mark the nuclear fraction. Percentage of fraction loaded into each lane is given below; higher percent of less concentrated nuclear fractions were loaded to equalize total protein per lane. Native Scrib and Dlg are found in both cytoplasmic and nuclear fractions of disc cells (C), but endogenously GFP-tagged Lgl is detected only in cytoplasmic and not nuclear fraction (D). Dlg is still found in both the nuclear and cytoplasmic fractions of *scrib* null samples, but in *dlg* null samples, Scrib is detected only in the cytoplasmic fraction (E). We note that in different experimental replicates, the relative cytoplasmic:nuclear ratio of Scrib protein is variable.

we infer that the amount of nuclear Dlg is small compared with that found in the cytoplasm. Because Dlg, Scrib, and Lgl colocalize at the cortex and work together in many biological contexts, we asked if either Scrib or Lgl were also found in the nuclear fraction. Western blotting of fractions showed a nuclear population of Scrib (Figure 2C), but not Lgl (Figure 2D). In *dlg* null flies, this nuclear population of Scrib was lost (Figure 2E). However, in *scrib* null flies, Dlg was still found in the nuclear fraction (Figure 2E). We therefore conclude that Dlg enters the nucleus independent of Scrib and that it is required for Scrib's nuclear localization, similar to the relationship between

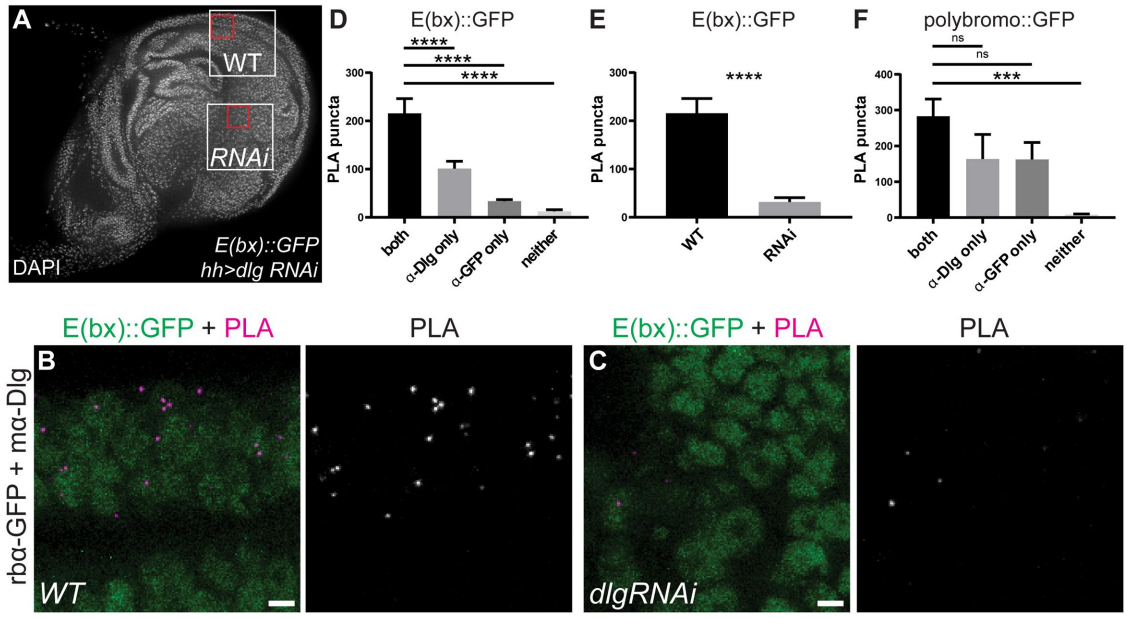

FIGURE 3: Nuclear Dlg can be detected in vivo in proximity to E(bx). (A) *E(bx)::GFP* wing disc nuclei expressing *UAS-dlg-RNAi* in the posterior compartment under control of *hhGAL4,* used for PLA. Yellow boxes indicate wild-type and *dlg* knockdown areas where signal in D, E was quantified. Red boxes indicate regions shown in B, C. (B) PLA from wild-type region; note that nearly all signal is within nuclei marked by E(bx)::GFP. Scale bar = 10 μM. (C) PLA from *dlg* RNAi region shows nearly no signal. Scale bar = 10 μM. (D) PLA signal is significantly increased between E(bx)::GFP and Dlg in WT tissue with both antibodies compared with samples with a single antibody or neither antibody. Graph displays mean with error bars of SEM. Ordinary one-way ANOVA. For ****, $p < 0.0001$. For both, $n = 14$ wing discs; α-Dlg only, $n = 15$ wing discs; α-GFP only, $n = 15$ wing discs; neither, $n = 12$ wing discs. (E) PLA signal is significantly increased between E(bx)::GFP and Dlg in wild-type tissue compared with *dlg* RNAi tissue. Graph displays mean with error bars of SEM. Paired, two-tailed t-test. For ****, $p < 0.0001$. $n = 14$ wing discs. (F) There is no significant PLA signal between Polybromo::GFP and Dlg compared with single antibody background. Graph displays mean with error bars of SEM. Ordinary one-way ANOVA. For ns, $p > 0.05$. For ***, $p = 0.0001$. For both, $n = 16$ wing discs; α-Dlg only, $n = 13$ wing discs; α-GFP only, $n = 13$ wing discs; neither, $n = 16$ wing discs.

the proteins at the cell cortex (Bilder *et al.*, 2000; Albertson and Doe, 2003; Khoury and Bilder, 2020; Ventura *et al.*, 2020).

Nuclear Dlg is in close proximity to the NURF complex

Having identified the existence of a small nuclear pool of Dlg, we considered what its function could be. In addition to "nucleus" and "nuclear pore," proteins associated with the term "chromatin remodeling complex" were also enriched in the APEX2-Dlg proteomic dataset (Figure 2, A and B). While several chromatin remodeling complexes were overrepresented in the proteomics dataset, for only one were all members of the complex present: the NURF complex (Figure 2, A and B; Supplemental Table S3).

The NURF complex is a conserved molecular machine that catalyzes, through an ATP-dependent mechanism, the sliding of nucleosomes along DNA to regulate gene expression (Badenhorst *et al.*, 2002; Bouazoune and Brehm, 2006; Alkhatib and Landry, 2011; Kwon *et al.*, 2016). In *Drosophila*, NURF is made up of four proteins: Imitation SWI (Iswi), Caf1-55, Nurf-38 and Enhancer of bithorax (E[bx]) (aka NURF301) (Xiao *et al.*, 2001; Alkhatib and Landry, 2011). E(bx) serves as a scaffold for the other three proteins. The NURF complex does not inherently possess sequence-specific DNA binding activity. Instead, it moves particular nucleosomes on specific target genes by binding to transcriptional regulatory proteins that themselves have DNA sequence specificity (Xiao *et al.*, 2001; Alkhatib and Landry, 2011; Kwon *et al.*, 2016). For example, the *Drosophila* NURF complex binds the GAGA transcription factor Trithorax-like (Trl) to move nucleosomes out of promoter regions—including those of Yki target genes—thereby facilitating transcriptional activation (Alkhatib and Landry, 2011; Oh *et al.*, 2013; Kwon *et al.*, 2016).

The APEX2 proteomic data suggest that Dlg is found within 20 nm of the NURF complex. To verify this, we turned to a proximity ligation assay (PLA) which creates a punctate fluorescent signal when two target proteins are less than 40 nm apart (Söderberg *et al.*, 2006). We performed PLA using α-Dlg and α-GFP antibodies on wing discs expressing the NURF complex member E(bx) endogenously tagged with GFP. We further expressed *dlg* RNAi in the posterior compartment of the E(bx)::GFP wing discs (Figure 3A) as an internal negative control for specificity. A positive PLA signal was detected in epithelial cells from the control side of wing discs (Figure 3B) that was significantly greater than single antibody background signal (Figure 3D) and also significantly greater than signal from the *dlg*-depleted portion of the discs (Figure 3, C and E). As a final control, we performed PLA on wing discs expressing Polybromo endogenously tagged with GFP. Polybromo is a member of the PBAP complex, one of two SWI/SNF chromatin remodeling complexes in *Drosophila* (Bouazoune and Brehm, 2006). We detected other SWI/SNF complex members in our MS data (Supplemental Tables S2 and S3) including Brm and Bap60 (Figure 2B), but not Polybromo. We therefore reasoned that Polybromo::GFP would be a stringent negative control. We did not detect PLA signal significantly above single antibody background between Dlg and Polybromo::GFP (Figure 3F).

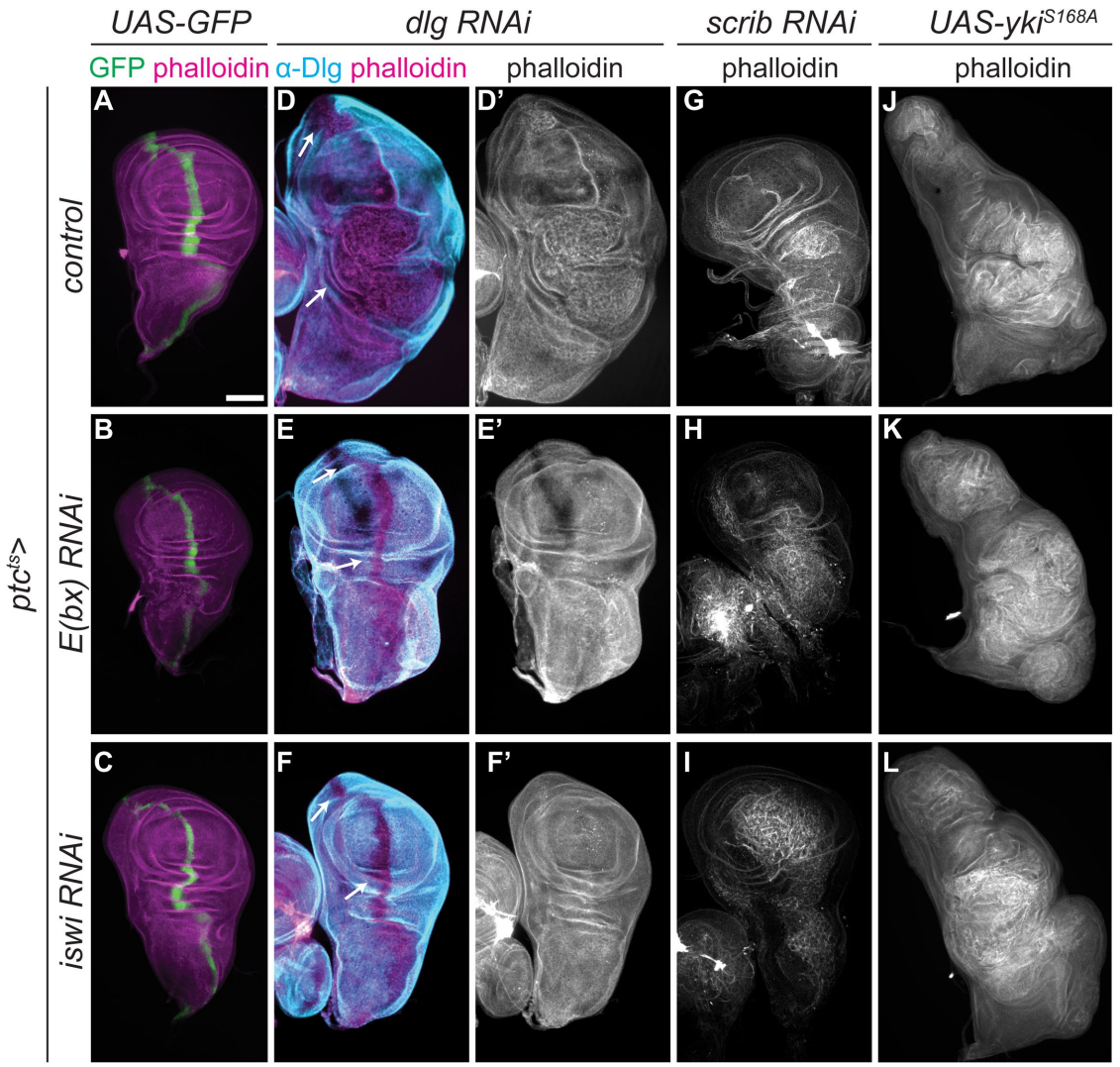

FIGURE 4: Overgrowth of *dlg*-depleted epithelia requires NURF complex. (A–C) *ptc*^{ts}*GAL4* drives expression of GFP along the AP compartment boundary (A). Discs expressing RNAi against NURF complex members *E(bx)* (B) or *iswi* (C) in the Ptc stripe have normal size and morphology. (D–F) Depleting *dlg* in the Ptc stripe caused neoplastic overgrowth in both proximal and distal hinge regions (D, arrows). Overgrowth was rescued by either *E(bx)* RNAi (E) or *iswi* RNAi (F). (G–I) Depleting *scrib* with RNAi in the Ptc stripe also caused neoplastic tumors (G), but tumor formation and growth were unaffected by coexpression of either *E(bx)* (H) or *iswi* (I) RNAi. (J–L) Expressing the constitutively active YkiS168A mutant in the Ptc stripe caused hyperplastic overgrowth of wing discs (J). Yki-driven overgrowth was unaffected by coexpression of either *E(bx)* (K) or *iswi* (L) RNAi. Scale bar = 100 μM.

An advantage of PLA in this context is its sensitivity, which allows small numbers of protein molecules to be visualized via microscopy with good spatial resolution. The PLA signal detected between Dlg and E(bx)::GFP appeared in the nuclei of epithelial cells (Figure 3B). Because Dlg has a well-established role in regulating spindle orientation during cell division (Albertson and Doe, 2003; Johnston *et al.*, 2009; Bergstralh *et al.*, 2013; Nakajima *et al.*, 2019), we considered that the nuclear Dlg signal from both MS and cell fractionation could derive exclusively from dividing cells. However, the PLA signal was even across cells and not limited to those undergoing mitosis. Thus, in addition to confirming a population of Dlg near the NURF complex, this method also enabled the detection of endogenous Dlg in the nuclei of intact cells, for the first time to our knowledge. These data corroborate the evidence from MS and subcellular fractionation that a nuclear pool of Dlg exists and lies specifically near the NURF complex.

The NURF complex is required for overgrowth of *dlg* tumors

We next sought to determine if there was a functional connection between Dlg and the NURF complex. Depleting *dlg* with RNAi from the boundary between anterior and posterior compartments of the wing disc using a conditionally active *ptc*^{ts}*GAL4* (see *Methods*) can cause neoplastic overgrowth in the hinge regions both proximal and distal to the pouch; within the pouch, *dlg*-depleted cells undergo apoptosis likely due to cell competition (Figure 4D). Depleting the NURF complex components *E(bx)* or *iswi* in otherwise WT discs using *ptc*^{ts}*GAL4* has no effect on hinge cells and only minor effects, inducing limited apoptosis, in the pouch (Figure 4, A–C). Strikingly, coexpressing RNAi against either NURF complex component along with *dlg* RNAi rescued the overgrowth of *dlg*-depleted cells (Figure 4, E and F). Examination of cell death revealed that *dlg*-depleted cells coexpressing NURF complex RNAi did not have

significantly increased levels of apoptosis cells in either the hinge or the pouch compared with *dlg* RNAi alone (Supplemental Figure S2, A–G), demonstrating that rescue of *dlg* RNAi by NURF complex depletion is not due to synthetic lethality. A similar reduction of tumor size by RNAi against NURF components was seen when *dlg* was depleted in the posterior compartment of wing discs induced using *hhGAL4* (Supplemental Figure S3, D–F). Again with this driver, expressing either NURF RNAi alone had little effect on tissue size, although these animals showed a small developmental delay (Supplemental Figure S3, A–C). We noticed that NURF RNAi restores the architecture of cells depleted of *dlg* using *ptc^{ts}GAL4* but not using *hhGAL4.* The latter tumors overgrow more than the former, and previous work has shown that mitotic cells are particularly challenged by polarity remodeling (Bergstralh *et al.*, 2013; Ragkousi *et al.*, 2017; Moreira *et al.*, 2019; Osswald and Morais-de-Sá, 2019); moreover, increased cell divisions may dilute the store of Dlg protein translated prior to the onset of RNAi. Finally, we found that heterozygosity for a null allele of E(bx), *E(bx)$^{NURF301-4}$*, partially suppressed the frequency of the pouch fold (55.2%, compared with 96.3% for *dlg* RNAi alone) and hinge overgrowth phenotypes (15.8%, compared with 55.2% for *dlg* RNAi alone) in *dlg* RNAi wing discs using the *ptc^{ts}GAL4* model (Supplemental Figure S4, A–E).

We tested the specificity of the requirement of NURF complex for tumor growth. Coexpression of a control RNAi construct targeting RFP did not rescue *dlg* RNAi phenotypes, suggesting that the suppression we observed is not due to titration of GAL4 by multiple UAS transgenes (Supplemental Figure S5, A–C). A constitutively active form of Yki (S168A) induces strong hyperplastic overgrowth when expressed in the *ptc^{ts}GAL4* stripe (Figure 4J), but this growth was not rescued by *E(bx)* or *iswi* RNAi (Figure 4, K and L). Even though there is also a nuclear pool of Scrib (Figure 2, C and E), overgrowth in *scrib* RNAi tumors was also not rescued by RNAi against either NURF component, and we did not observe altered levels of apoptosis in the pouch or hinge of *scrib* RNAi cells codepleted for NURF components (Figure 4, G–I; Supplemental Figure S2, G–J). These results suggest that the reduction of tumor size by NURF RNAi is not a general characteristic of all tumors and the rescue we observe is specific to *dlg*.

NURF complex promotes Yki target-gene expression in *dlg* tumors

Transcriptional changes that drive neoplastic tumor growth in *Drosophila* are regulated by a signaling network involving JNK-mediated regulation of the Fos transcription factor and aPKC-mediated regulation of Yki (Kulshammer *et al.*, 2015; Atkins *et al.*, 2016). Because the NURF complex, via its interaction with Trl, participates in activation of Yki target genes (Oh *et al.*, 2013), we asked if this might account for NURF complex role in promoting *dlg* tumor growth. NURF RNAi-mediated suppression of *dlg*-depleted tumor growth did not rescue epithelial architecture, but it caused significant suppression of a reporter for Yki activity, *ex-LacZ* (McCartney *et al.*, 2000; Hamaratoglu *et al.*, 2006). While NURF RNAi alone had no effect on expression of *ex-LacZ* in otherwise WT tissue (Figure 5, A–C), *ex-LacZ* expression was reduced to normal levels in *dlg* RNAi tissue coexpressing either NURF RNAi (Figure 5, D–F). However, in *scrib* RNAi tumors, where overgrowth is not suppressed, *ex-LacZ* levels are unchanged by NURF RNAi (Figure 5, G–I). Thus, the ability of NURF RNAi to limit tumor overgrowth correlates with the extent to which it limits Yki target gene activation in that tumor type. The failure of NURF RNAi to reduce the overgrowth caused by Yki^{S168A} (Figure 4, J–L) suggests that the NURF complex is not absolutely required for Yki to drive proliferation, and that strong, constitutive activation of Yki can overcome an unfavorable chromatin environment to drive gene expression. Altogether, these data support a model where nuclear Dlg negatively regulates the NURF complex to limit Yki driven growth.

Nuclear localization of Dlg involves sequences outside of consensus nuclear localization signals (NLSs)

To explore a function for nuclear Dlg, we investigated potential NLSs. Prediction algorithms consistently identified two regions enriched in basic amino acids that are characteristic of recognized NLSs (Figure 6A). The first lies at the C-terminus of PDZ1, while the second is in the so-called E-F region at the N-terminus of the HOOK domain, which itself lies between the SH3 and GUK domains. Both are conserved in the human homolog hDlg1, and for the latter, experimental evidence consistent with an NLS has been demonstrated (McLaughlin *et al.*, 2002; Roberts *et al.*, 2007). Transgenic constructs have previously deleted either the E-F or the entire HOOK domain; each results in mutant Dlg proteins that show strongly increased nuclear localization visible by immunohistochemistry (Hough *et al.*, 1997; Lu *et al.*, 2021). Since these data indicate that the E-F region cannot constitute the sole NLS of Dlg, we mutated basic residues within the predicted NLSs in both the E-F region and the PDZ1 to alanine (Dlg$^{2XNLS>A}$, Figure 6A).

When overexpressed in *dlg* mutant discs or follicle cells, Dlg$^{2XNLS>A}$ had no detectable rescuing activity compared with expression of WT Dlg (Figure 6, B and C; Supplemental Figure S6, H–J). Both Dlg$^{2XNLS>A}$ and matched WT Dlg transgenic proteins exhibited membrane and cytoplasmic localization in disc and follicle cells (Figure 6, D and E; Supplemental Figure S6, A–D). Quantitation of membrane localization in follicle cells showed that, while Dlg$^{2XNLS>A}$ was enriched at the membrane (PM Index >1), its localization was reduced compared with WT Dlg (Supplemental Figure S6, A–D, G). We considered whether this might be due to disruption of electrostatic membrane binding, since the mutated residues in NLS2 of Dlg$^{2XNLS>A}$ partially overlap with a recently described membrane binding polybasic region (Figure 6A) (Lu *et al.*, 2021). However, localization was further reduced in *scrib*-depleted cells (Supplemental Figure S6, E–G), while Dlg constructs that lack electrostatic membrane binding are insensitive to *scrib* depletion (Lu *et al.*, 2021). Most importantly, to determine if mutation of both predicted NLS altered Dlg's ability to enter the nucleus, we carried out subcellular fractionation studies on protein extracted from imaginal discs. Dlg$^{2XNLS>A}$ protein could still be detected in the nuclear fraction, similarly to the matched overexpressed WT Dlg (Figure 6F). We conclude that nuclear entry of Dlg can involve sequences outside of the two predicted NLSs.

DISCUSSION

Here we report the use of an in vivo proximity-based biotin labeling approach to investigate new biological functions of the polarity-regulating tumor suppressor Dlg. Our strategy used transgenic replacement of Dlg by an APEX2-tagged version, coupled with MS of subsequently tagged proteins; critically, we carried this out in native epithelial tissue. The resultant MS data led to the discovery of a nuclear pool of native Dlg that is not apparent by microscopy but that nevertheless lies near the NURF chromatin remodeling complex. We further found that NURF is required for the overgrowth of epithelia lacking Dlg and suggest that this may be due to the role of NURF in activating pro-proliferative *yki* target genes.

To our knowledge, our data provide the first demonstration of endogenous *Drosophila* Dlg in the nucleus. Dlg is a member of the membrane-associated guanylate kinase (MAGUK) family of

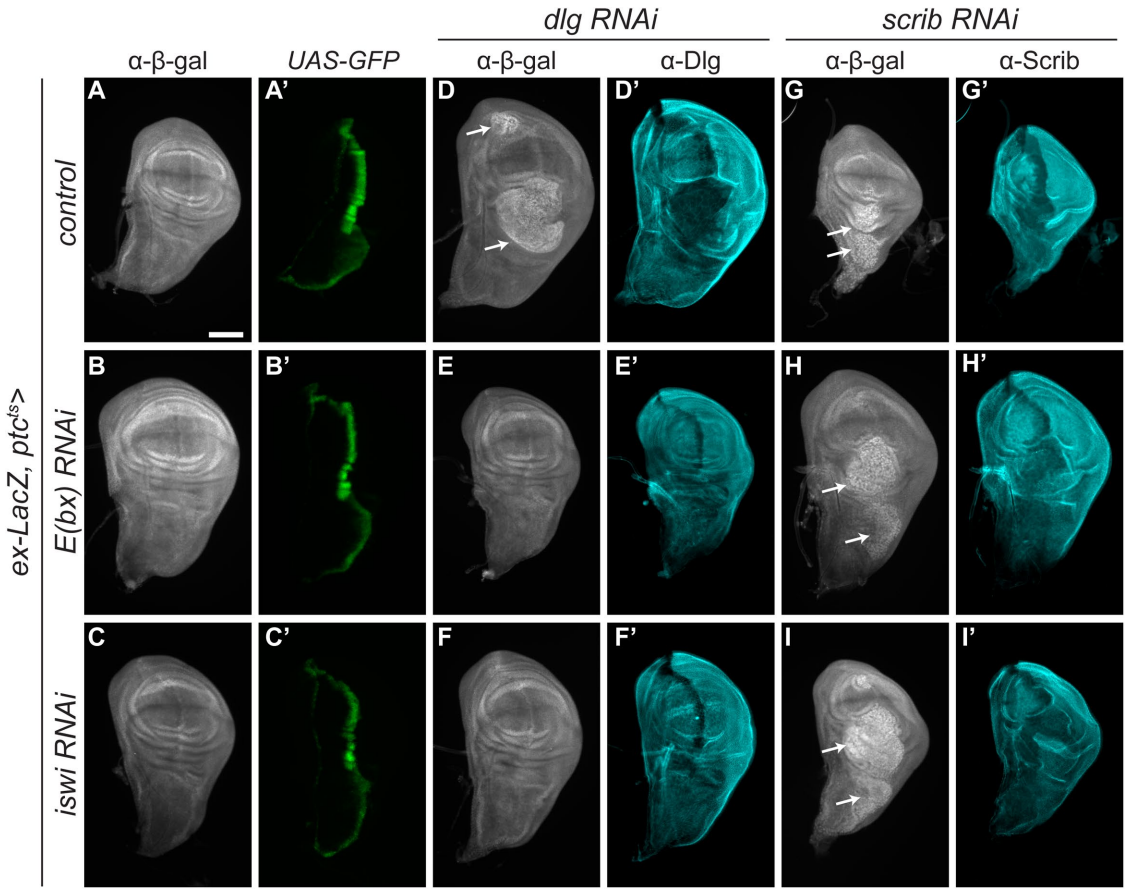

FIGURE 5: NURF RNAi rescues Yki target gene expression in *dlg* tumors. (A–C) *ex-LacZ* expression (α-β-gal) in control wing discs (A) was unaffected by either *E(bx)* (B) or *iswi* (C) RNAi. (D–F) *ex-LacZ* levels were elevated in neoplastically overgrown regions of *dlg* RNAi discs. (D, arrows). *E(bx)* (E) or *iswi* (F) RNAi coexpression rescued both overgrowth and *ex-LacZ* levels. (G–I) *ex-LacZ* levels were also elevated in neoplastically overgrown areas of *scrib* RNAi discs (G). Neither overgrowth nor *ex-LacZ* levels were rescued with coexpression of *E(bx)* (H) or *iswi* (I) RNAi. The phenotype here was made less severe than in Figure 4, G–I by reducing *ptc^tsGAL4* activity time, to facilitate comparison of normal to tumorous tissue. Scale bar = 100 μM.

proteins that are generally found at cell–cell junctions, but nuclear localization of many MAGUKs has also been observed including hDlg1 (Mantovani and Banks, 2003; Roberts *et al.*, 2007; Narayan *et al.*, 2009) as well as ZO-1 (Gottardi *et al.*, 1996; González-Mariscal *et al.*, 1999), ZO-2 (Islas *et al.*, 2002), CASK1 (Hsueh *et al.*, 2000), MAGI-2 (Dobrosotskaya *et al.*, 1997), and Nagie Oko (Bit-Avragim *et al.*, 2008). Due to their size, movement of MAGUKs into and out of the nucleus must involve active transport via NLS and nuclear export signals (NES) respectively, consistent with the presence of several importin proteins as well as the nuclear import regulator Ran in our Dlg proximity biotinylation dataset (Supplemental Tables S1 and S2). The predicted NLS in the Dlg E-F/HOOK region is conserved in hDlg1. The SH3-HOOK-GUK region undergoes an intramolecular interaction that regulates exposure of sequences that can mediate several Dlg functions (Nix *et al.*, 2000; McGee *et al.*, 2001; Qian and Prehoda, 2006; Marcette *et al.*, 2009; Newman and Prehoda, 2009; Zeng *et al.*, 2017; Rademacher *et al.*, 2019; Lu *et al.*, 2021); the increased nuclear localization of transgenic Dlg or hDlg1 deleted for the GUK domain raises the possibility that nuclear entry could be one of these (Thomas *et al.*, 2000; Kohu *et al.*, 2002; Lu *et al.*, 2021). The predicted NLS in Dlg PDZ1 is conserved not only in hDlg1 but also in the MAGUKs ZO-1, ZO-2, and their *Drosophila* homolog Polychaetoid. We were unable to predict an NES, although such sequences have been detected in vertebrate ZO-1 (Islas *et al.*, 2002), ZO-2 (Islas *et al.*, 2002; Jaramillo *et al.*, 2004; González-Mariscal *et al.*, 2006), and Nagie Oko (Bit-Avragim *et al.*, 2008). However, various transgenically expressed truncations of Dlg localize strongly to nuclei (Hough *et al.*, 1997; Thomas *et al.*, 2000; Bachmann *et al.*, 2004; Lu *et al.*, 2021), including one that deletes the E-F region itself. Additionally, coding exons that are alternatively spliced in a neural-specific isoform of Dlg are sufficient to drive nuclear localization; these protein sequences are conserved with hDlg1 (Bachmann *et al.*, 2004). Clearly, MAGUKs have evolved and maintained multiple mechanisms of nuclear entry and exit; our data demonstrate that this may be true even for proteins where a nuclear pool is not visible by microscopy.

We attempted to test the nuclear function of *Drosophila* Dlg by mutating two conserved and predicted NLSs; however, this failed to abolish nuclear entry. This result agrees with a recently published Dlg transgene that deletes the three PDZ domains while also mutating 15 basic residues in and adjacent to the predicted E-F region NLS to glutamine; nuclear localization of the mutant protein is visible, again emphasizing that an additional NLS must reside outside of the consensus sequences (Lu *et al.*, 2021). Interestingly, Dlg$^{2XNLS>A}$ provided no rescuing activity, consistent with the deleterious effects of mutations in the HOOK domain (Hough *et al.*, 1997; Lu *et al.*,

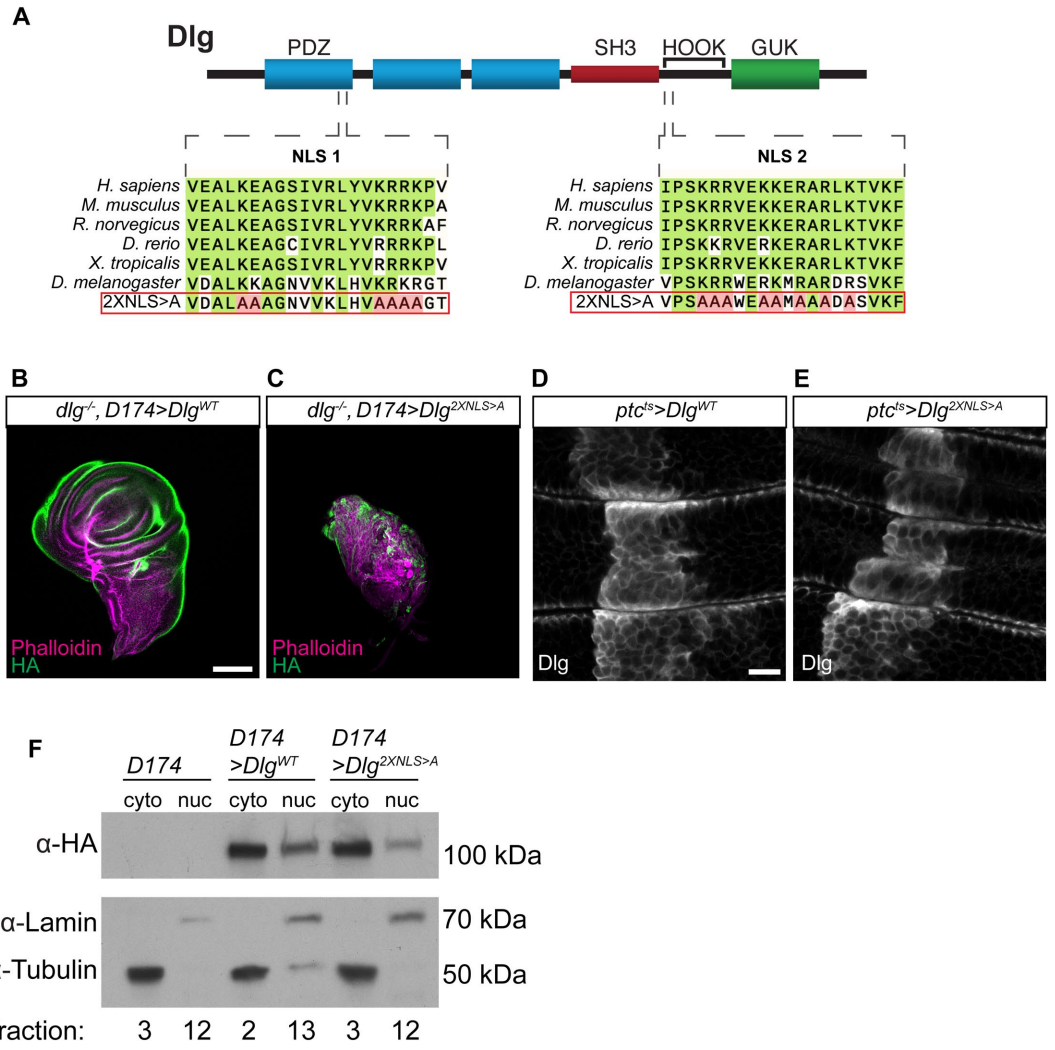

FIGURE 6: Dlg nuclear localization involves sequences outside of predicted NLSs. (A) Diagram of Dlg protein, with predicted NLS shown in relation to conserved domains. Conservation of NLSs is shown in alignment of Dlg homologues. Mutations in $Dlg^{2XNLS>A}$ are shown in red. (B, C) *dlg* null mutant wing discs are rescued by expression of Dlg^{WT} (B) but not $Dlg^{2XNLS>A}$ (C). (D, E) Localization of Dlg^{WT} (D) under *ptc-GAL4* is comparable to $Dlg^{2XNLS>A}$ (E), although the latter shows more cytoplasmic staining. Transgenes are detected by anti-Dlg staining: compare to endogenous protein localization neighboring the stripe. (F) Western blots of fractionated disc extracts expressing transgenic Dlg proteins, detected by α-HA. Blots are also probed with Tubulin (α-tub) to mark the cytoplasmic fraction and Lamin (α-lam) to mark the nuclear fraction. Dlg^{WT} and $Dlg^{2XNLS>A}$ are both found in the nuclear as well as the cytoplasmic fraction. Scale bars in B and C = 100 μM and in D and E = 10 μM.

2021). Previous work shows that PDZ and GUK domains are not absolutely required for Dlg function, while the SH3 and HOOK domains are (Hough *et al.*, 1997; Thomas *et al.*, 2000; Khoury and Bilder, 2020; Lu *et al.*, 2021). Our results hint at a critical role for the eight basic amino acids in the E-F region within HOOK that is independent of electrostatic membrane binding; these can be the subject of future experiments.

Nakajima and Gibson recently used coimmunoprecipitation (Co-IP) to isolate Dlg-associated proteins from embryos. Their dataset identified several proteins involved in nuclear pore traffic (Ran, CRM1, NUP358) but not NURF components (Nakajima *et al.*, 2019). Similarly, we were unable to Co-IP Dlg and NURF complex member E(bx) (data not shown). It is possible that Dlg and E(bx) associate through an interaction that is not stable enough to pull down or that Dlg may interact with another member of the NURF complex (for which reagents for co-IP were not available) or through an intermediary protein. Any of these possibilities would highlight the utility of APEX2 fusion proteins to facilitate the in vivo detection of weak and/or transient interactions that are hard to discover by other methods. In the case of the Scrib module, they could provide a path forward to identifying relevant interactors, which has been a major obstacle in understanding the biology of these key polarity-regulating tumor suppressors.

It has long been observed that Scrib, Dlg, and Lgl are required to maintain the proper transcriptional state of epithelial tissues (Hariharan and Bilder, 2006; Grzeschik *et al.*, 2010; Zhu *et al.*, 2010; Doggett *et al.*, 2011; Sun and Irvine, 2011; Bunker *et al.*, 2015). Our observations that Dlg is near the NURF complex in the nucleus and that the NURF complex is required for Yki-driven overgrowth of *dlg* tumors suggest that Dlg may regulate transcription through a much more direct mechanism than previously thought. Several other MAGUKs physically interact with transcription factors, including ZO-2

with Jun, Fos, C/EBP (Betanzos *et al.*, 2004), Myc (Huerta *et al.*, 2007), YAP (Oka *et al.*, 2010) (the vertebrate homolog of Yki), and TEAD (Gallego-Gutiérrez *et al.*, 2021), while CASK1 can form a trimeric complex in the nucleus with the T-box transcription factor Tbr-1 and CINAP, a nucleosome assembly protein that facilitates chromatin remodeling (Hsueh *et al.*, 2000; Wang *et al.*, 2004).

While we found a functional role for the NURF complex in tumor overgrowth in *dlg* mutants, the same assays did not produce evidence for a functional connection between the NURF complex and the Scrib. This is intriguing, given the close relationship between Scrib and Dlg in epithelial polarity and our evidence here that Scrib is also detectable in the nucleus. However, it is clear that Scrib and Dlg do not have overlapping functions (Elsum *et al.*, 2012; Stephens *et al.*, 2018); recent work has demonstrated distinct roles for the two proteins, in part by showing that they cannot substitute for one another in epithelial polarity (Khoury and Bilder, 2020; Ventura *et al.*, 2020). Independent roles have also been documented for the *Caenorhabditis elegans* Scrib and Dlg homologues (Legouis *et al.*, 2000; Firestein and Rongo, 2001; McMahon *et al.*, 2001), and recent proteomic studies in *C. elegans* as well as *Drosophila* uncover only modestly overlapping sets of Scrib- and Dlg-interacting proteins (Waaijers *et al.*, 2016; Nakajima *et al.*, 2019) (reviewed in Stephens *et al.*, 2018). Of particular relevance here, transcriptome profiling of *scrib* and *dlg* mutant wing disc tumors also found only partially overlapping changes in gene expression (Bunker *et al.*, 2015). It is therefore plausible that while Dlg may regulate transcription via the NURF complex, Scrib's effects on gene expression may be exerted in a distinct manner. Whether these effects require nuclear entry of Scrib will await further study.

The association between nuclear *Drosophila* Dlg and the NURF complex extends data about other nuclear MAGUKs and supports the importance of this understudied aspect of these highly conserved proteins. Still, as we were unable to separately test the functions of cytoplasmic and nuclear Dlg pools, we cannot definitively conclude that the latter drives the observed growth phenotypes. We also do not know how Dlg proteins move through the pore; whether the nuclear population is a small, stable pool or a transient, dynamic one; or the signals or cellular states that cause their nuclear localization. Nonetheless, our data indicate that a comprehensive understanding of this critical protein may have to include its function not just at the PM but also in the nucleus.

METHODS

Request a protocol through *Bio-protocol*.

Drosophila stocks and genetics

Drosophila melanogaster stocks were raised on cornmeal molasses food. Experimental crosses were raised at 25°C unless otherwise noted. Fly lines used are listed in Supplemental Table S4; *ptc^{ts}GAL4* denotes the use of *ptcGAL4* in combination with temperature-sensitive GAL80 (GAL80ts) to allow conditional GAL4 expression on temperature shift. For experiments using *ptc^{ts}GAL4*, crosses were started at 25°C. Adults were removed after 48 h then after another 24 h, vials were shifted to 29°C to induce Gal4 expression. Wing discs were dissected from wandering third-instar larvae starting 72 h after temperature shift and continuing every 24 h thereafter for 1–3 additional days to track tumor development. For clonal GAL4 expression in follicle cells, larvae were heat-shocked for 13 min at 37°C 120 h after egg deposition (AED). For follicle cell MARCM experiments, larvae were heat-shocked for 1 h on 3 consecutive days starting at 120 h AED. Ovaries were dissected from adult females fed on yeast for 3 d after eclosion. The sequences for *UAS-3xMyc-APEX2-Dlg, UAS-Dlg-3xHA,* and *UAS-Dlg$^{2XNLS>A}$-3xHA* are presented in Supplemental Table S4. *UAS-3xMyc-APEX2-Dlg* contains the *dlgA* coding sequence with the *dlg S97*-specific exon using a cDNA provided by Ulrich Thomas; it was cloned into a Gateway N-terminal *3xMyc-APEX2* destination vector. *UAS-Dlg-3xHA* was cloned into the *pUAST-attB* vector and contains a C-terminal flexible linker followed by a 3xHA tag. *UAS-Dlg$^{2XNLS>A}$-3xHA* was cloned from *UAS-Dlg-3xHA* using Gibson assembly (NEB). All transgenes were inserted into the *attP40* site. Primer sequences are given in Supplemental Table S4.

Immunofluorescence and microscopy

Wandering third-instar larval imaginal discs were dissected in phosphate-buffered saline (PBS) and fixed for 20 min in 4% paraformaldehyde (PFA). Samples were rinsed in PBS. Follicles were dissected in Schneider's medium containing 15% fetal bovine serum (FBS) and fixed for 20 min in 4% PFA. Primary and secondary antibodies were diluted in PBST (0.1% Triton X-100) with 4% NGS (Life Technologies) and 1% bovine serum albumin (BSA; Life Technologies). Primary antibodies (Supplemental Table S4) were incubated with samples overnight at 4°C. Secondary fluorophore–conjugated antibodies (Molecular Probes) were diluted 1:400 and incubated for 2 h at room temperature. Phalloidin and DAPI incubated with samples for 20 min in PBS. Images were captured on a Zeiss LSM700 scanning confocal microscope or a Zeiss Axio Imager M2 with Apotome 2 with Plan Apochromat 20×/NA 0.8, LD C-Apochromat 40×/NA 1.1 W and Plan Apochromat 63×/NA 1.4 oil objectives at 1024 × 1024 pixels with 2 line averages.

For all imaginal disc experiments, at least 15 discs were examined per condition, except in Supplemental Figure S3, H and I, where 7 discs were analyzed per genotype. For follicle cell experiments, tissue from at least 5 females was analyzed and at least 10 ovarioles and at least 2 egg chambers per ovariole were examined. Images are representative of at least 2 independent biological replicates. Reported phenotypes were observed with at least 80% penetrance in all cases unless otherwise noted.

Dlg cortical enrichment was quantified as described in Lu *et al.* (2021). For single cells in en face confocal sections, the fluorescent signal intensity of at the membrane and in the cytoplasm were quantified in Fiji (Schindelin *et al.*, 2012) using rectangular ROIs of fixed 1.17 µM width, approximately the thickness of the cell cortex. The ratio of membrane:cytoplasmic intensity was calculated to give the "PM index." Average PM indices were calculated for all cells per genotype.

Death caspase-1 enrichment was quantified by taking the mean fluorescence intensity in maximum intensity projected images of a 63.77 µM-wide rectangular ROI spanning the *ptc^{ts}GAL4*-expressing stripe and an adjacent, equivalently sized control ROI outside the GAL4 domain and calculating the ratio of these two values per disc. Ratios were calculated separately for the wing pouch and the hinge.

Western blots

Protein concentrations in samples were measured by BCA protein assay (Pierce). Proteins were electrophoresed at 150 V for 1 h through 7.5% or 4–20% mini-PROTEAN TGX gels (Bio-Rad) and blotted at 300 mA for 1 h onto PVDF membranes. Membranes were blocked in 3% BSA in Tris-buffered saline (TBS)-T for 1 h. All antibodies were incubated with membrane in blocking solution. Primary antibodies were incubated overnight at 4°C. Streptavidin-HRP and HRP–conjugated secondary antibodies were incubated with the membrane for 2 h at room temperature. Blots were developed with standard ECL reagents (Advansta).

Sample preparation and biotin labeling for mass spectrometry

Larvae were reared at room temperature (21–23°C). Thoracic discs were dissected in chilled labeling media: Schneider's medium (Life Technologies) containing 1% Pen/Strep (Caisson Labs), 10% FBS (Life Technologies), 500 µM biotin-phenol (aka biotinyl tyramide, AdipoGen Life Sciences), and 2 mM probenecid (Thermo). Samples were incubated at room temperature with nutation for 30 min. Labeling media was removed. Samples were incubated in 1 mM hydrogen peroxide for 1 min. Samples were then washed three times in quenching buffer (5 mM Trolox [Sigma], 10 mM sodium azide [Sigma], and 10 mM sodium ascorbate [Sigma] in PBS) and three times in PBS. Samples were lysed in RIPA buffer (50 mM Tris-HCl, pH 8.0, 150 mM NaCl, 1% NP-40, 0.5% sodium deoxycholate, 0.1% SDS, and protease inhibitors [Pierce mini-tablets]) using a pellet pestle motor and a polypropylene pestle. All solutions were pre-chilled on ice. Lysates were spun at 14,000 rpm in a tabletop microfuge for 10 min at 4°C to remove debris, and supernatants were saved as final sample lysate. A 5-µl lysate sample was reserved for Western blot analysis. The remainder was incubated with streptavidin–conjugated magnetic beads (Pierce) for 1 h at room temperature. Beads were washed twice in TBS with 0.1% Tween20, then three times with RIPA buffer. For Western blot analysis of pull down of biotinylated proteins, beads were boiled for 5 min in 60 µl SDS–PAGE sample buffer: NuPAGE LDS buffer (Thermo) with 20 mM DTT (Sigma) and 2 mM biotin (Thermo). Supernatant was saved as eluate 1 (E1). Beads were then boiled for 5 min in 40 µl sample buffer and supernatant was saved as eluate 2 (E2). For MS, labeled lysates were prepared in batches and stored at –80°C until all samples had been collected. Samples were then thawed and pooled into three replicates from 400 larvae each, and biotinylated proteins were isolated as described above. Protein-bound beads were kept in PBS at 4°C. MS, including remaining sample prep, was performed by the UC Davis Mass Spectrometry Facilities.

Proteins on beads were received and the buffer was exchanged with four washes of 50 mM TEAB (triethylammonium bicarbonate). The proteins were then digested off the beads overnight with trypsin at room temperature. The following day, the supernatant was removed, and the beads were washed with 50 mM TEAB and pooled with the supernatant. The peptides in all six sample were quantified using Pierce fluorescent peptide assay (Thermo Scientific).

TMT labeling

Based on the fluorescent peptide assay, the volume for 20 µg of the most concentrated sample was determined, and equal volumes of each sample were diluted with 50 mM TEAB to 25 µl per replicate. Each sample was labeled with TMT 6 Plex Mass Tag Labeling Kit (Thermo Scientific). Briefly, 20 µl of each TMT label (126-131) was added to each digested peptide sample and incubated for an hour. The reaction was quenched with 1 µl of 5% hydroxylamine and incubated for 15 min. All labeled samples were then mixed together and lyophilized to almost dryness. The TMT-labeled sample was reconstituted in 2% acetonitrile 0 0.1% TFA and desalted with a zip tip.

LC-MS3

LC separation was done on a Dionex nano Ultimate 3000 (Thermo Scientific) with a Thermo Easy-Spray source. The digested peptides were reconstituted in 2% acetonitrile/0.1% trifluoroacetic acid, and 5 µl of each sample was loaded onto a PepMap 100 Å 3U 75 µm × 20 mm reverse-phase trap where they were desalted online before being separated on a 100 Å 2U 50 µm × 150 mm PepMap EasySpray reverse-phase column. Peptides were eluted using a 90-min gradient of 0.1% formic acid (A) and 80% acetonitrile (B) with a flow rate of 200 nl/min. The separation gradient was run with 2–5% B over 1 min, 5–10% B over 9 min, 10–20% B over 27 min, 20–35% B over 10 min, 35–99% B over 10 min, a 2-min hold at 99% B, and finally 99–2% B held at 2% B for 5 min.

MS3 synchronous precursor selection (SPS) workflow

Mass spectra were collected on a Fusion Lumos mass spectrometer (Thermo Fisher Scientific) in a data-dependent MS3 SPS method. MS1 spectra were acquired in the Orbitrap, 120 K resolution, 50 ms max inject time, 5 × 105 max inject time. MS2 spectra were acquired in the linear ion trap with a 0.7 Da isolation window, CID fragmentation energy of 35%, turbo scan speed, 50 ms max inject time, 1 × 104 AGC, and maximum parallelizable time turned on. MS2 ions were isolated in the ion trap and fragmented with an HCD energy of 65%. MS3 spectra were acquired in the orbitrap with a resolution of 50 K and a scan range of 100–500 Da, 105 ms max inject time, and 1 × 105 AGC.

MS3 SPS workflow

Database searching: tandem mass spectra were extracted by Proteome Discoverer 2.2. Charge state deconvolution and deisotoping were not performed. All MS/MS samples were analyzed using SequestHT (XCorr Only) (Thermo Fisher Scientific, San Jose, CA) in Proteome Discoverer 2.2.0.388. Sequest (XCorr Only) was set up to search uniprot-proteome-3AUP000000803.fasta (unknown version, 21,134 entries) and an equal number of decoy sequences, assuming the digestion enzyme trypsin. Sequest (XCorr Only) was searched with a fragment ion mass tolerance of 0.60 Da and a parent ion tolerance of 10.0 PPM. Carbamidomethyl of cysteine and TMT6plex of lysine were specified in Sequest (XCorr Only) as fixed modifications. Deamidated of asparagine, oxidation of methionine and acetyl of the n-terminus were specified in Sequest (XCorr Only) as variable modifications.

Criteria for protein identification: Scaffold (version Scaffold_4.8.4, Proteome Software, Portland, OR) was used to validate MS/MS-based peptide and protein identifications. Peptide identifications were accepted if they could be established at greater than 74.0% probability to achieve a false discovery rate (FDR) less than 1.0% by the Scaffold Local FDR algorithm. Protein identifications were accepted if they could be established at greater than 35.0% probability to achieve an FDR less than 1.0% and contained at least two identified peptides. This resulted in a peptide decoy FDR of 0.31% and a Protein Decoy FDR of 0.8%. Protein probabilities were assigned by the Protein Proph*et al*gorithm (Nesvizhskii *et al*., 2003). Proteins that contained similar peptides and could not be differentiated based on MS/MS analysis alone were grouped to satisfy the principles of parsimony. Proteins sharing significant peptide evidence were grouped into clusters.

Quantitative data analysis: Scaffold Q+ (version Scaffold_4.8.4, Proteome Software, Portland, OR) was used to quantitate label-based quantitation (TMT) peptide and protein identifications. Peptide identifications were accepted if they could be established at greater than 74.0% probability to achieve an FDR less than 1.0% by the Scaffold Local FDR algorithm. Protein identifications were accepted if they could be established at greater than 35.0% probability to achieve an FDR less than 1.0% and contained at least two identified peptides. Protein probabilities were assigned by the Protein Proph*et al*gorithm (Nesvizhskii *et al*., 2003). Proteins that contained similar peptides and could not be differentiated based on MS/MS analysis alone were grouped to satisfy the principles of

parsimony. Proteins sharing significant peptide evidence were grouped into clusters. Channels were corrected by correction factors supplied by the manufacturer in all samples according to the algorithm described in i-Tracker (Shadforth *et al.*, 2005). Normalization was performed iteratively (across spectra) on intensities, as described in the statistical analysis of relative labeled mass spectrometry data from complex samples using anova (Oberg *et al.*, 2008). Medians were used for averaging. Spectra data were log-transformed, pruned of those matched to multiple proteins, and weighted by an adaptive intensity weighting algorithm. Of 3635 spectra in the experiment at the given thresholds, 3247 (89%) were included in quantitation. Differentially expressed proteins were determined by applying the permutation test with unadjusted significance level $p < 0.05$ corrected by Benjamini-Hochberg.

Data availability

Raw data, mzML, and Scaffold results are available from the MassIVE proteomics repository (MSV000087186) and Proteome Exchange (PXD025378).

GO analysis

Cellular component GO analysis was performed using the BiNGO plug-in for Cytoscape using all genes in the *D. melanogaster* genome as a reference set. User selected settings were as follows: hypergeometric statistical test; Benjamini-Hochberg FDR used to correct *P* values; significance level set to 0.05.

Multiple sequence alignment

Multiple sequence alignment of Dlg NLS sequences was made with Clustal Omega (Madeira *et al.*, 2019). Aligned sequences were visualized using SnapGene Viewer. The following protein sequences were used: *Homo sapiens*, UniProt Q12959; *Mus musculus*, UniProt Q811D0; *Rattus norvegicus*, UniProt Q62696; *Danio rerio*, UniProt E7FAT1; *Xenopus tropicalis*, UniProt Q28C55; *D. melanogaster*, UniProt P31007.

Subcellular fractionation

Sixty to 70 wandering third-instar larvae were dissected in PBS. Cells were lysed using five strokes with the small pestle in a Dounce homogenizer in 10 mM HEPES, pH 7.6, 10 mM KCl, 1.5 mM $MgCl_2$, 0.5 mM DTT, and 0.05% NP-40. After homogenization, samples were incubated on ice for 10 min and then spun at 3000 rpm for 10 min in a tabletop microfuge. Supernatant was spun at 14,000 × *g* for 10 min and supernatant was cytoplasmic fraction. Pellet from the first spin was rinsed in PBS. Pellet was then resuspended in 5 mM HEPES, pH 7.6, 1.5 mM $MgCl_2$, 300 mM NaCl, 0.2 mM EDTA, and 26% glycerol. Nuclei in resuspended pellet were lysed by 20 strokes with the large pestle of a Dounce homogenizer. Sample was incubated on ice for 30 min and then spun at 24,000 × *g* for 20 min. Supernatant was nuclear fraction. All buffers were prechilled on ice and contained protease inhibitors (Pierce). All spins were conducted at 4°C.

PLA

PLA was performed using a Duolink In Situ Orange Mouse/Rabbit Kit (Sigma) according to the manufacturer's instructions with the following modifications. Samples were dissected and fixed as for immunofluorescence. Tissue was permeabilized in PBST, then washed 3× in PBS before proceeding. All subsequent steps were performed in recommended volumes in tubes with mounting of samples onto slides as the final step. Confocal images were taken on a Zeiss LSM 700 scanning microscope. For quantification, the total number of PLA puncta were counted in a maximum projection of a 101.61 × 101.61 × 24 µm vol from two regions of each disc: control and *dlg* RNAi. Presented images are a maximum projection of 5 µM depth. Images were processed and analyzed in Fiji. Statistics were done in Prism.

Statistical methods

Statistical significance was determined using two tailed *t* test or one-way ANOVA with Tukey's multiple comparisons test. Analysis of mass spec data is described above in "MS3 SPS Workflow" and used Permutation Test with unadjusted significance level $p < 0.05$ corrected by Benjamini-Hochberg. GO analysis is described above and used hypergeometric test with Benjamini-Hochberg FDR to correct *P* values; significance level set to 0.05. In figures, n.s. is $P > 0.05$, $*p < 0.05$, $**p < 0.01$, $***p < 0.001$, and $****p < 0.0001$.

ACKNOWLEDGMENTS

We thank Laura Mathies for cloning *Dlg*$^{2XNLS>A}$, Norbert Perrimon for key reagents, the UC Davis Core Proteomics facility for assistance, and the Bilder lab for helpful discussions. LC-MS was supported by a National Institutes of Health (NIH) shared instrumentation Grant S10OD021801. This work was supported by NIH Grants R01 GM090150 and R35 GM130388 to D.B., American Heart Association (AHA) Postdoctoral Fellowship 17POST33660155 to K.A.S., and AHA Predoctoral Fellowship 20PRE35120150 to M.J.K.

REFERENCES

Albertson R, Doe CQ (2003). Dlg, Scrib and Lgl regulate neuroblast cell size and mitotic spindle asymmetry. Nat Cell Biol 5, 166–170.

Alkhatib SG, Landry JW (2011). The Nucleosome Remodeling Factor. FEBS Lett 585, 3197–3207.

Amacher JF, Brooks L, Hampton TH, Madden DR (2020). Specificity in PDZ-peptide interaction networks: Computational analysis and review. J Struct Biol X 4, 100022.

Anastas JN, Biechele TL, Robitaille M, Muster J, Allison KH, Angers S, Moon RT (2012). A protein complex of SCRIB, NOS1AP and VANGL1 regulates cell polarity and migration, and is associated with breast cancer progression. Oncogene 31, 3696–3708.

Atkins M, Potier D, Romanelli L, Jacobs J, Mach J, Hamaratoglu F, Aerts S, Halder G (2016). An ectopic network of transcription factors regulated by hippo signaling drives growth and invasion of a malignant tumor model. Curr Biol 26, 714–723.

Audebert S, Navarro C, Nourry C, Chasserot-Golaz S, Lécine P, Bellaiche Y, Dupont JL, Premont RT, Sempéré C, Strub JM, *et al.* (2004). Mammalian scribble forms a tight complex with the βPIX exchange factor. Curr Biol 14, 987–995.

Bachmann A, Timmer M, Sierralta J, Pietrini G, Gundelfinger ED, Knust E, Thomas U (2004). Cell type-specific recruitment of Drosophila Lin-7 to distinct MAGUK-based protein complexes defines novel roles for Sdt and Dlg-S97. J Cell Sci 117, 1899–1909.

Badenhorst P, Voas M, Rebay I, Wu C (2002). Biological functions of the ISWI chromatin remodeling complex NURF. Genes Dev 16, 3186–3198.

Bagci H, Sriskandarajah N, Robert A, Boulais J, Elkholi IE, Tran V, Lin ZY, Thibault MP, Dubé N, Faubert D, *et al.* (2020). Mapping the proximity interaction network of the Rho-family GTPases reveals signalling pathways and regulatory mechanisms. Nat Cell Biol 22, 120–134.

Baumgartner R, Stocker H, Hafen E (2013). The RNA-binding proteins FMR1, rasputin and caprin act together with the UBA protein lingerer to restrict tissue growth in Drosophila melanogaster. PLoS Genet 9, e1003598.

Belotti E, Polanowska J, Daulat AM, Audebert S, Thomé V, Lissitzky JC, Lembo F, Blibek K, Omi S, Lenfant N, *et al.* (2013). The human PDZome: A gateway to PSD95-disc large-zonula occludens (PDZ)-mediated functions. Mol Cell Proteomics 12, 2587–2603.

Bergstralh DT, Lovegrove HE, St Johnston D (2013). Discs large links spindle orientation to apical-basal polarity in drosophila epithelia. Curr Biol 23, 1707–1712.

Betanzos A, Huerta M, Lopez-Bayghen E, Azuara E, Amerena J, González-Mariscal L (2004). The tight junction protein ZO-2 associates with Jun, Fos and C/EBP transcription factors in epithelial cells. Exp Cell Res 292, 51–66.

Bilder D (2004). Epithelial polarity and proliferation control: Links from the Drosophila neoplastic tumor suppressors. Genes Dev 18, 1909–1925.
Bilder D, Li M, Perrimon N (2000). Cooperative regulation of cell polarity and growth by Drosophila tumor suppressors. Science 289, 113–116.
Bilder D, Schober M, Perrimon N (2003). Integrated activity of PDZ protein complexes regulates epithelial polarity. Nat Cell Biol 5, 53–58.
Bit-Avragim N, Rohr S, Rudolph F, Van Der Ven P, Fürst D, Eichhorst J, Wiesner B, Abdelilah-Seyfried S (2008). Nuclear localization of the zebrafish tight junction protein nagie oko. Dev Dyn 237, 83–90.
Bouazoune K, Brehm A (2006). ATP-dependent chromatin remodeling complexes in Drosophila. Chromosom Res 14, 433–449.
Bunker BD, Nellimoottil TT, Boileau RM, Classen AK, Bilder D (2015). The transcriptional response to tumorigenic polarity loss in Drosophila. Elife 2015.
Campanale JP, Sun TY, Montell DJ (2017). Development and dynamics of cell polarity at a glance. J Cell Sci 130.
Van Campenhout CA, Eitelhuber A, Gloeckner CJ, Giallonardo P, Gegg M, Oller H, Grant SGN, Krappmann D, Ueffing M, Lickert H (2011). Dlg3 Trafficking and apical tight junction formation is regulated by Nedd4 and Nedd4-2 E3 Ubiquitin ligases. Dev Cell 21, 479–491.
Caruana G, Bernstein A (2001). Craniofacial dysmorphogenesis including cleft palate in mice with an insertional mutation in the discs large gene. Mol Cell Biol 21, 1475.
Chen C-L, Hu Y, Udeshi ND, Lau TY, Wirtz-Peitz F, He L, Ting AY, Carr SA, Perrimon N (2015). Proteomic mapping in live Drosophila tissues using an engineered ascorbate peroxidase. Proc Natl Acad Sci USA 112, 12093–12098.
Choi J, Troyanovsky RB, Indra I, Mitchell BJ, Troyanovsky SM (2019). Scribble, Erbin, and Lano redundantly regulate epithelial polarity and apical adhesion complex. J Cell Biol 218, 2277–2293.
Dash BP, Schnöder TM, Kathner C, Mohr J, Weinert S, Herzog C, Godavarthy PS, Zanetti C, Perner F, Braun-Dullaeus R, *et al.* (2018). Diverging impact of cell fate determinants Scrib and Llgl1 on adhesion and migration of hematopoietic stem cells. J Cancer Res Clin Oncol 144, 1933–1944.
Dobrosotskaya I, Guy RK, James GL (1997). MAGI-1, a membrane-associated guanylate kinase with a unique arrangement of protein–protein interaction domains. J Biol Chem 272, 31589–31597.
Doggett K, Grusche FA, Richardson HE, Brumby AM (2011). Loss of the Drosophila cell polarity regulator Scribbled promotes epithelial tissue overgrowth and cooperation with oncogenic Ras-Raf through impaired Hippo pathway signaling. BMC Dev Biol 11, 57.
Drew K, Lee C, Huizar RL, Tu F, Borgeson B, McWhite CD, Ma Y, Wallingford JB, Marcotte EM (2017). Integration of over 9,000 mass spectrometry experiments builds a global map of human protein complexes. Mol Syst Biol 13, 932.
Elsum I, Yates L, Humbert PO, Richardson HE (2012). The Scribble-Dlg-Lgl polarity module in development and cancer: From flies to man. Essays Biochem 53, 141–168.
Firestein BL, Rongo C (2001). DLG-1 is a MAGUK similar to SAP97 and is required for adherens junction formation. Mol Biol Cell 12, 3465–3475.
Gallego-Gutiérrez H, González-González L, Ramírez-Martínez L, López-Bayghen E, González-Mariscal L (2021). Tight junction protein ZO-2 modulates the nuclear accumulation of transcription factor TEAD. Mol Biol Cell 32, mbc.E20-07-0470.
Gingras A-C, Abe KT, Raught B (2019). Getting to know the neighborhood: using proximity-dependent biotinylation to characterize protein complexes and map organelles. Curr Opin Chem Biol 48, 44–54.
González-Mariscal L, Islas S, Contreras RG, García-Villegas MR, Betanzos A, Vega J, Diaz-Quiñónez A, Martín-Orozco N, Ortiz-Navarrete V, Cereijido M, *et al.* (1999). Molecular characterization of the tight junction protein ZO-1 in MDCK cells. Exp Cell Res 248, 97–109.
González-Mariscal L, Ponce A, Alarcón L, Jaramillo BE (2006). The tight junction protein ZO-2 has several functional nuclear export signals. Exp Cell Res 312, 3323–3335.
Gottardi CJ, Arpin M, Fanning AS, Louvard D (1996). The junction-associated protein, zonula occludens-1, localizes to the nucleus before the maturation and during the remodeling of cell-cell contacts. Proc Natl Acad Sci USA 93, 10779–10784.
Grzeschik NA, Parsons LM, Allott ML, Harvey KF, Richardson HE (2010). Lgl, aPKC, and crumbs regulate the salvador/warts/hippo pathway through two distinct mechanisms. Curr Biol 20, 573–581.
Halaoui R, McCaffrey L (2015). Rewiring cell polarity signaling in cancer. Oncogene 34, 939–950.
Hamaratoglu F, Willecke M, Kango-Singh M, Nolo R, Hyun E, Tao C, Jafar-Nejad H, Halder G (2006). The tumour-suppressor genes NF2/Merlin and Expanded act through Hippo signalling to regulate cell proliferation and apoptosis. Nat Cell Biol 8, 27–36.
Hariharan IK, Bilder D (2006). Regulation of imaginal disc growth by tumor-suppressor genes in Drosophila. Annu Rev Genet 40, 335–361.
Hough CD, Woods DF, Park S, Bryant PJ (1997). Organizing a functional junctional complex requires specific domains of the Drosophila MAGUK Discs large. Genes Dev 11, 3242–3253.
Hsueh Y-P, Wang T-F, Yang F-C, Sheng M (2000). Nuclear translocation and transcription regulation by the membrane-associated guanylate kinase CASK/LIN-2. Nature 404, 298–302.
Huerta M, Muñoz R, Tapia R, Soto-Reyes E, Ramírez L, Recillas-Targa F, González-Mariscal L, López-Bayghen E (2007). Cyclin D1 is transcriptionally down-regulated by ZO-2 via an E box and the transcription factor c-Myc. Mol Biol Cell 18, 4826–4836.
Humbert PO, Grzeschik NA, Brumby AM, Galea R, Elsum I, Richardson HE (2008). Control of tumourigenesis by the Scribble/Dlg/Lgl polarity module. Oncogene 27, 6888–6907.
Hung V, Udeshi ND, Lam SS, Loh KH, Cox KJ, Pedram K, Carr SA, Ting AY (2016). Spatially resolved proteomic mapping in living cells with the engineered peroxidase APEX2. Nat Protoc 11, 456–475.
Hung V, Zou P, Rhee H-W, Udeshi ND, Cracan V, Svinkina T, Carr SA, Mootha VK, Ting AY (2014). Proteomic mapping of the human mitochondrial intermembrane space in live cells via ratiometric APEX tagging. Mol Cell 55, 332–341.
Iizuka-Kogo A, Ishidao T, Akiyama T, Senda T (2007). Abnormal development of urogenital organs in Dlgh1-deficient mice. Development 134, 1799–1807.
Islas S, Vega J, Ponce L, González-Mariscal L (2002). Nuclear localization of the tight junction protein ZO-2 in epithelial cells. Exp Cell Res 274, 138–148.
Van Itallie CM, Aponte A, Tietgens AJ, Gucek M, Fredriksson K, Anderson JM (2013). The N and C termini of ZO-1 are surrounded by distinct proteins and functional protein networks. J Biol Chem 288, 13775–13788.
Ivarsson Y, Arnold R, McLaughlin M, Nim S, Joshi R, Ray D, Liu B, Teyra J, Pawson T, Moffat J, *et al.* (2014). Large-scale interaction profiling of PDZ domains through proteomic peptide-phage display using human and viral phage peptidomes. Proc Natl Acad Sci USA 111, 2542–2547.
Izumi Y, Furuse M (2014). Molecular organization and function of invertebrate occluding junctions. Semin Cell Dev Biol 36, 186–193.
Jaramillo BE, Ponce A, Moreno J, Betanzos A, Huerta M, Lopez-Bayghen E, Gonzalez-Mariscal L (2004). Characterization of the tight junction protein ZO-2 localized at the nucleus of epithelial cells. Exp Cell Res 297, 247–258.
Johnston CA, Hirono K, Prehoda KE, Doe CQ (2009). Identification of an Aurora-A/PinsLINKER/dlg spindle orientation pathway using induced cell polarity in S2 cells. Cell 138, 1150–1163.
Khoury MJ, Bilder D (2020). Distinct activities of Scrib module proteins organize epithelial polarity. Proc Natl Acad Sci 117, 11531–11540.
Koh YH, Popova E, Thomas U, Griffith LC, Budnik V (1999). Regulation of DLG localization at synapses by CaMKII-dependent phosphorylation. Cell 98, 353–363.
Kohu K, Ogawa F, Akiyama T (2002). The SH3, HOOK and guanylate kinase-like domains of hDLG are important for its cytoplasmic localization. Genes to Cells 7, 707–715.
Kulshammer E, Mundorf J, Kilinc M, Frommolt P, Wagle P, Uhlirova M (2015). Interplay among Drosophila transcription factors Ets21c, Fos and Ftz-F1 drives JNK-mediated tumor malignancy. DMM Dis Model Mech 8, 1279–1293.
Kwon SY, Grisan V, Jang B, Herbert J, Badenhorst P (2016). Genome-wide mapping targets of the metazoan chromatin remodeling factor NURF reveals nucleosome remodeling at enhancers, core promoters and gene insulators. PLOS Genet 12, e1005969.
Lam SS, Martell JD, Kamer KJ, Deerinck TJ, Ellisman MH, Mootha VK, Ting AY (2014). Directed evolution of APEX2 for electron microscopy and proximity labeling. Nat Methods 12, 51–54.
Lee SR, Hong ST, Choi KW (2020). Regulation of epithelial integrity and organ growth by Tctp and Coracle in Drosophila. PLoS Genet 16, e1008885.
Legouis R, Gansmuller A, Sookhareea S, Bosher JM, Baillie DL, Labouesse M (2000). LET-413 is a basolateral protein required for the assembly of adherens junctions in *Caenorhabditis elegans*. Nat Cell Biol 2, 415–422.
Lizama CO, Zovein AC (2013). Polarizing pathways: Balancing endothelial polarity, permeability, and lumen formation. Exp Cell Res 319, 1247–1254.

Lu J, Dong W, Tao Y, Hong Y (2021). Electrostatic plasma membrane targeting contributes to Dlg function in cell polarity and tumorigenesis. Development dev.196956.
Madeira F, Park YM, Lee J, Buso N, Gur T, Madhusoodanan N, Basutkar P, Tivey ARN, Potter SC, Finn RD, *et al.* (2019). The EMBL-EBI search and sequence analysis tools APIs in 2019. Nucleic Acids Res 47, W636–W641.
Mannix KM, Starble RM, Kaufman RS, Cooley L (2019). Proximity labeling reveals novel interactomes in live Drosophila tissue. Development 146, dev176644.
Mantovani F, Banks L (2003). Regulation of the discs large tumor suppressor by a phosphorylation-dependent interaction with the β-TrCP ubiquitin ligase receptor. J Biol Chem 278, 42477–42486.
Marcette J, Hood IV, Johnston CA, Doe CQ, Prehoda KE (2009). Allosteric control of regulated scaffolding in membrane-associated guanylate kinases. Biochemistry 48, 10014–10019.
Martell JD, Deerinck TJ, Sancak Y, Poulos TL, Mootha VK, Sosinsky GE, Ellisman MH, Ting AY (2012). Engineered ascorbate peroxidase as a genetically encoded reporter for electron microscopy. Nat Biotechnol 30, 1143–1148.
McCartney BM, Kulikauskas RM, LaJeunesse DR, Fehon RG (2000). The neurofibromatosis-2 homologue, Merlin, and the tumor suppressor expanded function together in Drosophila to regulate cell proliferation and differentiation. Development 127, 1315–1324.
McGee AW, Dakoji SR, Olsen O, Bredt DS, Lim WA, Prehoda KE (2001). Structure of the SH3-guanylate kinase module from PSD-95 suggests a mechanism for regulated assembly of MAGUK scaffolding proteins. Mol Cell 8, 1291–1301.
McLaughlin M, Hale R, Ellston D, Gaudet S, Lue RA, Viel A (2002). The distribution and function of alternatively spliced insertions in hDlg. J Biol Chem 277, 6406–6412.
McMahon L, Legouis R, Vonesch JL, Labouesse M (2001). Assembly of C. elegans apical junctions involves positioning and compaction by LET-413 and protein aggregation by the MAGUK protein DLG-1. J Cell Sci 114, 2265–2277.
Michaelis UR, Chavakis E, Kruse C, Jungblut B, Kaluza D, Wandzioch K, Manavski Y, Heide H, Santoni MJ, Potente M, *et al.* (2013). The polarity protein scrib is essential for directed endothelial cell migration. Circ Res 112, 924–934.
Moreira S, Osswald M, Ventura G, Gonçalves M, Sunkel CE, Morais-de-Sá E (2019). PP1-mediated dephosphorylation of Lgl controls apical-basal polarity. Cell Rep 26, 293–301.
Nagasaka K, Seiki T, Yamashita A, Massimi P, Subbaiah VK, Thomas M, Kranjec C, Kawana K, Nakagawa S, Yano T, *et al.* (2013). A Novel Interaction between hScrib and PP1γ downregulates ERK signaling and suppresses oncogene-induced cell transformation. PLoS One 8, 1–10.
Nakajima Y, Lee ZT, McKinney SA, Swanson SK, Florens L, Gibson MC (2019). Junctional tumor suppressors interact with 14-3-3 proteins to control planar spindle alignment. J Cell Biol, jcb.201803116.
Narayan N, Subbaiah VK, Banks L (2009). The high-risk HPV E6 oncoprotein preferentially targets phosphorylated nuclear forms of hDlg. Virology 387, 1–4.
Nechiporuk T, Fernandez TE, Vasioukhin V (2007). Failure of epithelial tube maintenance causes hydrocephalus and renal cysts in Dlg5-/- Mice. Dev Cell 13, 338–350.
Nesvizhskii AI, Keller A, Kolker E, Aebersold R (2003). A statistical model for identifying proteins by tandem mass spectrometry. Anal Chem 75, 4646–4658.
Newman RA, Prehoda KE (2009). Intramolecular interactions between the Src homology 3 and guanylate kinase domains of discs large regulate its function in asymmetric cell division. J Biol Chem 284, 12924–12932.
Nix SL, Chishti AH, Anderson JM, Walther Z (2000). hCASK and hDlg associate in epithelia, and their Src homology 3 and guanylate kinase domains participate in both intramolecular and intermolecular interactions. J Biol Chem 275, 41192–41200.
Oberg AL, Mahoney DW, Eckel-Passow JE, Malone CJ, Wolfinger RD, Hill EG, Cooper LT, Onuma OK, Spiro C, Therneau TM, Bergen HR III (2008). Statistical analysis of relative labeled mass spectrometry data from complex samples using ANOVA. J Proteome Res 7, 225–233.
Oh H, Slattery M, Ma L, Crofts A, White KP, Mann RS, Irvine KD (2013). Genome-wide association of Yorkie with chromatin and chromatin-remodeling complexes. Cell Rep 3, 309–318.
Oka T, Remue E, Meerschaert K, Vanloo B, Boucherie C, Gfeller D, Bader GD, Sidhu SS, Vandekerckhove J, Gettemans J, *et al.* (2010). Functional complexes between YAP2 and ZO-2 are PDZ domain-dependent, and regulate YAP2 nuclear localization and signalling1. Biochem J 432, 461–478.
Oshima K, Fehon RG (2011). Analysis of protein dynamics within the septate junction reveals a highly stable core protein complex that does not include the basolateral polarity protein Discs large. J Cell Sci 124, 2861–2871.
Osswald M, Morais-de-Sá E (2019). Dealing with apical–basal polarity and intercellular junctions: a multidimensional challenge for epithelial cell division. Curr Opin Cell Biol 60, 75–83.
Portela M, Yang L, Paul S, Li X, Veraksa A, Parsons LM, Richardson HE (2018). Lgl reduces endosomal vesicle acidification and Notch signaling by promoting the interaction between Vap33 and the V-ATPase complex. Sci Signal 11, eaar1976.
Qian Y, Prehoda KE (2006). Interdomain interactions in the tumor suppressor discs large regulate binding to the synaptic protein GukHolder. J Biol Chem 281, 35757–35763.
Rademacher N, Kuropka B, Kunde S-A, Wahl MC, Freund C, Shoichet SA (2019). Intramolecular domain dynamics regulate synaptic MAGUK protein interactions. Elife 8.
Ragkousi K, Marr K, Mckinney S, Ellington L, Gibson MC, Ragkousi K, Marr K, Mckinney S, Ellington L, Gibson MC (2017). Cell-cycle-coupled oscillations in apical polarity and intercellular contact maintain order in embryonic epithelia. Curr Biol, 1–6.
Rhee H-W, Zou P, Udeshi ND, Martell JD, Mootha VK, Carr SA, Ting AY (2013). Proteomic mapping of mitochondria in living cells via spatially restricted enzymatic tagging. Science 339, 1328–1331.
Roberts S, Calautti E, Vanderweil S, Nguyen HO, Foley A, Baden HP, Viel A (2007). Changes in localization of human discs large (hDlg) during keratinocyte differentiation is associated with expression of alternatively spliced hDlg variants. Exp Cell Res 313, 2521–2530.
Rodriguez-Boulan E, Macara IG (2014). Organization and execution of the epithelial polarity programme. Nat Rev Mol Cell Biol 15, 225–242.
Schindelin J, Arganda-Carreras I, Frise E, Kaynig V, Longair M, Pietzsch T, Preibisch S, Rueden C, Saalfeld S, Schmid B, *et al.* (2012). Fiji: An open-source platform for biological-image analysis. Nat Methods 9, 676–682.
Shadforth IP, Dunkley TP, Lilley KS, Bessant C (2005). i-Tracker: For quantitative proteomics using iTRAQ. BMC Genomics 61, 1–6.
Siegrist SE, Doe CQ (2005). Microtubule-induced pins/Gαi cortical polarity in Drosophila neuroblasts. Cell 123, 1323–1335.
Söderberg O, Gullberg M, Jarvius M, Ridderstråle K, Leuchowius KJ, Jarvius J, Wester K, Hydbring P, Bahram F, Larsson LG, *et al.* (2006). Direct observation of individual endogenous protein complexes in situ by proximity ligation. Nat Methods 3, 995–1000.
Stephens R, Lim K, Portela M, Kvansakul M, Humbert PO, Richardson HE (2018). The Scribble Cell Polarity Module in the Regulation of Cell Signaling in Tissue Development and Tumorigenesis. J Mol Biol 430, 3585–3612.
Su W-H, Mruk DD, Wong EWP, Lui W-Y, Cheng CY (2012). Polarity protein complex Scribble/Lgl/Dlg and epithelial cell barriers. Adv Exp Med Biol 763, 149–170.
Sun G, Irvine KD (2011). Regulation of Hippo signaling by Jun kinase signaling during compensatory cell proliferation and regeneration, and in neoplastic tumors. Dev Biol 350, 139–151.
Tan B, Yatim SMJM, Peng S, Gunaratne J, Hunziker W, Ludwig A (2020). The Mammalian Crumbs Complex Defines a Distinct Polarity Domain Apical of Epithelial Tight Junctions. Curr Biol, 1–14.
Tepass U, Tanentzapf G (2001). Epithelial cell polarity and cell junctions in Drosophila. Annu Rev Genet 35, 747–784.
Thomas U, Ebitsch S, Gorczyca M, Koh YH, Hough CD, Woods D, Gundelfinger ED, Budnik V (2000). Synaptic targeting and localization of Discs-large is a stepwise process controlled by different domains of the protein. Curr Biol 10, 1108–1117.
Trinkle-Mulcahy L (2019). Recent advances in proximity-based labeling methods for interactome mapping. F1000Research 8, 135.
Ventura G, Moreira S, Barros-Carvalho A, Osswald M, Morais-de-Sá E (2020). Lgl cortical dynamics are independent of binding to the Scrib-Dlg complex but require Dlg-dependent restriction of aPKC. Development dev.186593.
Waaijers S, Muñoz J, Berends C, Ramalho JJ, Goerdayal SS, Low TY, Zoumaro-Djayoon AD, Hoffman M, Koorman T, Tas RP, *et al.* (2016). A tissue-specific protein purification approach in Caenorhabditis elegans identifies novel interaction partners of DLG-1/Discs large. BMC Biol 14, 66.

Wang G-S, Hong C-J, Yen T-Y, Huang H-Y, Ou Y, Huang T-N, Jung W-G, Kuo T-Y, Sheng M, Wang T-F, *et al.* (2004). Transcriptional modification by a CASK-interacting nucleosome assembly protein. Neuron 42, 113–128.
Woods DF, Hough C, Peel D, Callaini G, Bryant PJ (1996). Dig protein is required for junction structure, cell polarity, and proliferation control in Drosophila Epithelia. J Cell Biol 134, 1469–1482.
Worzfeld T, Schwaninger M (2016). Apicobasal polarity of brain endothelial cells. J Cereb Blood Flow Metab 36, 340–362.
Xiao H, Sandaltzopoulos R, Wang H-M, Hamiche A, Ranallo R, Lee K-M, Fu D, Wu C (2001). Dual functions of largest NURF subunit NURF301 in nucleosome sliding and transcription factor interactions. Mol Cell 8, 531–543.
Zarnescu DC, Jin P, Betschinger J, Nakamoto M, Wang Y, Dockendorff TC, Feng Y, Jongens TA, Sisson JC, Knoblich JA, *et al.* (2005). Fragile X protein functions with Lgl and the PAR complex in flies and mice. Dev Cell 8, 43–52.
Zeng M, Ye F, Xu J, Zhang M (2017). PDZ ligand binding-induced conformational coupling of the PDZ-SH3-GK tandems in PSD-95 family MAGUKs. J Mol Biol 430, 69–86.
Zhu M, Xin T, Weng S, Gao Y, Zhang Y, Li Q, Li M (2010). Activation of JNK signaling links lgl mutations to disruption of the cell polarity and epithelial organization in Drosophila imaginal discs. Cell Res 20, 242–245.